SLAC-PUB-12781
astro-ph/0708.2750
August 2007

The Sloan Digital Sky Survey-II Supernova Survey: Search Algorithm and Follow-up Observations

Masao Sako,[1,2] Bruce Bassett,[3,4] Andrew Becker,[5] David Cinabro,[6] Fritz DeJongh,[7] D. L. Depoy,[8] Ben Dilday,[9,10] Mamoru Doi,[11] Joshua A. Frieman,[7,9,12] Peter M. Garnavich,[13] Craig J. Hogan,[14] Jon Holtzman,[15] Saurabh Jha,[2] Richard Kessler,[9,16] Kohki Konishi,[17] Hubert Lampeitl,[18] John Marriner,[7] Gajus Miknaitis,[7] Robert C. Nichol,[19] Jose Luis Prieto,[8] Adam G. Reiss,[18,20] Michael W. Richmond,[21] Roger Romani,[2,22] Donald P. Schneider,[23] Mathew Smith,[19] Mark SubbaRao,[12] Naohiro Takanashi,[11] Kouichi Tokita,[11] Kurt van der Heyden,[4] Naoki Yasuda,[17] Chen Zheng,[2,22] John Barentine,[24,25] Howard Brewington,[25] Changsu Choi,[26] Jack Dembicky,[25] Michael Harnavek,[25] Yutaka Ihara,[27] Myungshin Im,[26] William Ketzeback,[25] Scott J. Kleinman,[25,28] Jurek Krzesiński,[25,29] Daniel C. Long,[25] Elena Malanushenko,[25] Viktor Malanushenko,[25] Russet J. McMillan,[25] Tomoki Morokuma,[27,30] Atsuko Nitta,[25,31] Kaike Pan,[25] Gabrelle Saurage,[25] Stephanie A. Snedden[25]

Submitted to The Astronomical Journal

Work supported in part by US Department of Energy contract DE-AC02-76SF00515

KIPAC, SLAC, Stanford Univesity, Stanford, CA 94309

[1] Department of Physics and Astronomy, University of Pennsylvania, 209 South 33rd Street, Philadelphia, PA 19104.

[2] Kavli Institute for Particle Astrophysics & Cosmology, Stanford University, P.O. Box 20450, MS29, Stanford, CA 94309.

[3] Department of Mathematics and Applied Mathematics, University of Cape Town, Rondebosch 7701, South Africa.

[4] South African Astronomical Observatory, P.O. Box 9, Observatory 7935, South Africa.

[5] Department of Astronomy, University of Washington, Box 351580, Seattle, WA 98195.

[6] Department of Physics, Wayne State University, Detroit, MI 48202.

[7] Center for Particle Astrophysics, Fermi National Accelerator Laboratory, P.O. Box 500, Batavia, IL 60510.

[8] Department of Astronomy, Ohio State University, 140 West 18th Avenue, Columbus, OH 43210-1173.

[9] Kavli Institute for Cosmological Physics, The University of Chicago, 5640 South Ellis Avenue Chicago, IL 60637.

[10] Department of Physics, University of Chicago, Chicago, IL 60637.

[11] Institute of Astronomy, Graduate School of Science, University of Tokyo 2-21-1, Osawa, Mitaka, Tokyo 181-0015, Japan.

[12] Department of Astronomy and Astrophysics, The University of Chicago, 5640 South Ellis Avenue, Chicago, IL 60637.

[13] University of Notre Dame, 225 Nieuwland Science, Notre Dame, IN 46556-5670.

[14] Department of Astronomy, University of Washington, Box 351580, Seattle, WA 98195.

[15] Department of Astronomy, MSC 4500, New Mexico State University, P.O. Box 30001, Las Cruces, NM 88003.

[16] Enrico Fermi Institute, University of Chicago, 5640 South Ellis Avenue, Chicago, IL 60637.

[17] Institute for Cosmic Ray Research, University of Tokyo, 5-1-5, Kashiwanoha, Kashiwa, Chiba, 277-8582, Japan.

[18] Space Telescope Science Institute, 3700 San Martin Drive, Baltimore, MD 21218.

[19] Institute of Cosmology and Gravitation, Mercantile House, Hampshire Terrace, University of Portsmouth, Portsmouth PO1 2EG, UK.

[20] Department of Physics and Astronomy, Johns Hopkins University, 3400 North Charles Street, Baltimore, MD 21218.

[21] Physics Department, Rochester Institute of Technology, 85 Lomb Memorial Drive, Rochester, NY 14623-5603.

[22] Department of Physics, Stanford University, 382 Via Pueblo Mall, Stanford, CA 94305.

ABSTRACT

The Sloan Digital Sky Survey-II Supernova Survey has identified a large number of new transient sources in a 300 deg^2 region along the celestial equator during its first two seasons of a three-season campaign. Multi-band (*ugriz*) light curves were measured for most of the sources, which include solar system objects, Galactic variable stars, active galactic nuclei, supernovae (SNe), and other astronomical transients. The imaging survey is augmented by an extensive spectroscopic follow-up program to identify SNe, measure their redshifts, and study the physical conditions of the explosions and their environment through spectroscopic diagnostics. During the survey, light curves are rapidly evaluated to provide an initial photometric type of the SNe, and a selected sample of sources are targeted for spectroscopic observations. In the first two seasons, 476 sources were selected for spectroscopic observations, of which 403 were identified as SNe. For the Type Ia SNe, the main driver for the Survey, our photometric typing and targeting efficiency is 90%. Only 6% of the photometric SN Ia candidates were spectroscopically classified as non-SN Ia instead, and the remaining 4% resulted in low signal-to-noise, unclassified spectra. This paper describes the search algorithm and the software, and the real-time processing of the SDSS imaging data. We also present the details of the supernova candidate selection procedures and strategies for follow-up spectroscopic and imaging observations of the discovered sources.

Subject headings: cosmology: observations — methods: data analysis — tech-

---

[23] Department of Astronomy and Astrophysics, The Pennsylvania State University, 525 Davey Laboratory, University Park, PA 16802.

[24] Department of Astronomy, McDonald Observatory, University of Texas, Austin, TX 78712.

[25] Apache Point Observatory, P.O. Box 59, Sunspot, NM 88349.

[26] Department of Astronomy, Seoul National University, Seoul, South Korea.

[27] Institute of Astronomy, Graduate School of Science, University of Tokyo, 2-21-1, Osawa, Mitaka, Tokyo 181-0015, Japan.

[28] Subaru Telescope, 650 North A'ohoku Place, Hilo, HI 96720.

[29] Obserwatorium Astronomiczne na Suhorze, Akademia Pedagogicazna w Krakowie, ulica Podchorążych 2, PL-30-084 Kraków, Poland.

[30] National Observatory of Japan, 2-21-1, Osawa, Mitaka, Tokyo 181-8588, Japan.

[31] Gemini Observatory, 670 North A'ohoku Place, Hilo, HI 96720.

niques: image processing — supernovae: general — surveys

1. Introduction

Measurements of luminosity distances to Type Ia supernovae (SNe) have played a central role in cosmology, leading two independent groups to the remarkable discovery of an unknown, presently-dominant component of the universe, dark energy, and strong evidence for an accelerating universe (Riess et al. 1998; Perlmutter et al. 1999). Current surveys that target high-redshift SNe from the ground – the Canada-France-Hawaii Telescope Supernova Legacy Survey (SNLS[1]; Astier et al. 2006) and the Equation of State: Supernovae Trace Cosmic Expansion (ESSENCE[2]; Wood-Vasey et al. 2007; Miknaitis et al. 2007) – and from space using the *HST* (Riess et al. 2004a, 2007; Barbary et al. 2006) have substantially increased the sample of high-z SNe, and have provided much-improved statistical constraints on the expansion history of the universe.

The discovery of cosmic acceleration was made possible in part through extensive observations of nearby Type Ia SNe by the Calán/Tololo Supernova Search (Hamuy et al. 1993, 1996a,b,c) and by the CfA follow-up program (Riess et al. 1995; Riess 1996; Riess et al. 1999; Jha et al. 2006, 2007), and by studies pioneered by Pskovskii (1977) and by Phillips (1993) of the relationship between peak brightness and light curve decline rate (Hamuy et al. 1996d; Riess et al. 1996; Phillips et al. 1999). Current low-redshift SN surveys and follow-up programs (Lick Observatory Supernova Search – LOSS[3]; Filippenko et al. 2001, Carnegie Supernova Project – CSP[4]; Hamuy et al. 2006, Nearby Supernova Factory – SNFactory[5]; Aldering et al. 2002, and the CfA SN Group[6]), are continuing to discover SNe and compile a large number of high-quality multicolor light curves as well as multi-epoch optical spectra of SNe Ia to expand the library of local training data used as "templates". These high-quality data sets will be indispensable for calibrating the brightness-decline relation to high precision. Obtaining and studying multi-epoch spectra are also important for computing improved K-corrections and minimizing systematic uncertainties (Kim et al. 1996; Nugent et al. 2002;

[1]http://www.cfht.hawaii.edu/SNLS

[2]http://www.ctio.noao.edu/essence

[3]http://astro.berkeley.edu/b̃ait/kait.html

[4]http://csp1.lco.cl/ cspuser1/PUB/CSP.html

[5]http://snfactory.lbl.gov/

[6]http://cfa-www.harvard.edu/oir/Research/supernova/SNgroup.html

Hsiao et al. 2007). Recent spectroscopic modeling efforts have also led to a better understanding of the physical mechanism responsible for the observed brightness-decline relation (see, e.g., Kasen & Woosley 2007 and references therein).

As one of the three primary scientific components of the Sloan Digital Sky Survey-II (SDSS-II), the Supernova Survey takes repeated imaging scans of the same 300 square degrees of the sky during the Fall seasons of 2005 – 2007 to search for and measure light curves of SNe. The imaging survey is complemented by an extensive spectroscopic follow-up program to confirm the SN type and measure redshifts, and to study the detailed spectral properties of a sample of selected events.

This program exploits the unique capabilities of the SDSS 2.5m telescope (Gunn et al. 2006) and its CCD imaging camera (Gunn et al. 1998) to survey a large volume of space at moderately high cadence. The survey complements and improves upon other low-z and high-z surveys in several important ways. The wide field-of-view camera operating in drift scan mode allows for efficient discoveries of type Ia SNe at $0.05 \lesssim z \lesssim 0.4$, a redshift interval that is not easily probed by other existing surveys that target either known nearby galaxies (low-z) or narrow pencil-beam volumes (high-z). Its well-calibrated multi-band photometric system (*ugriz*; Fukugita et al. 1996) enables precise measurements of supernova light curves with controlled systematics. The absolute magnitude scale is accurate to better than $\sim 2\%$ in r and $\sim 2-3\%$ in the colors (Adelman-McCarthy et al. 2007), and a factor of ~ 2 improvement has been obtained from repeat imaging of the equatorial region (Ivezić et al. 2007). Finally, the survey is sensitive to the redshift interval that, given a large enough sample, enables cosmological distance measurements with data from a *single telescope*, eliminating the need for cross-calibration across two or more photometric systems.

This paper is part of a series describing the SDSS-II Supernova Survey. Here we present a technical description of the search algorithm, data processing, photometric typing of SN candidates, and spectroscopic target selection. Frieman et al. (2007) presents an overview of the program. Photometry and light curves of the full sample of spectroscopically confirmed SNe from the 2005 season are presented in Holtzman et al. (2007). Spectroscopic data and their analysis results are described in Zheng et al. (2007). Kessler et al. (2007) presents the SN Ia Hubble diagram and cosmological analysis from the 2005 season. The measurement of the low-redshift Type Ia SN rate is presented in Dilday et al. (2007). Detailed studies of two peculiar SNe discovered by the SDSS-II SN Survey, SN2005hk and SN2005gj, are presented in Phillips et al. (2007) and Prieto et al. (2007), respectively.

The main body of the paper is separated into two broad sections. The first part (§2) presents the details of the real-time on-mountain data processing and the mechanics of the search pipeline, which identifies new transient events. The second part (§3) describes the

procedures for supernova candidate identification, photometric SN typing, and the algorithm adopted for selecting targets for spectroscopy. A brief discussion of follow-up imaging observations of a sample of spectroscopically confirmed SNe is presented in §4. The general results from the 2005 and 2006 seasons are presented in §5. We briefly summarize in §6.

2. SDSS 2.5m Observations and Data Processing

The SDSS-II Supernova Survey has been allocated the bulk of the time during the Fall seasons (September 1 - November 30) of 2005 – 2007 on the SDSS telescope at Apache Point Observatory (APO). Imaging observations are scheduled on most nights excluding a 5-day period around full moon. Some nights are shared with the SEGUE program especially during stretches of consecutive nights with good observing conditions. An overview of the SDSS is given by York et al. (2000); see Frieman et al. (2007) for an overview of the SN Survey.

2.1. Survey Area: Stripe 82

The survey area is Stripe 82, the 300 deg^2 southern equatorial stripe of the SDSS footprint, which covers the approximate coordinate ranges $-60^\circ \lesssim \alpha \lesssim +60^\circ$ (20 hrs to 4 hrs in right ascension, RA or α) and $-1.25^\circ \lesssim \delta \lesssim +1.25^\circ$ in declination (δ). The detailed Stripe 82 footprint of each camera column is shown in Table 1. This survey area was selected for three primary reasons: (1) extensive repeat observations were acquired as part of the SDSS-I survey, before the start of the SN Survey, (2) the area is easily accessible to most telescopes, and (3) it is accessible at low airmass during the Fall months, when most of the northern SDSS area is not. The advantages of having repeat observations from SDSS-I are three-fold. First, the data provide a catalog of known variable sources, which is crucial for distinguishing a small number of new SN candidates from a large population of foreground variable stars and background active galactic nuclei. Second, the deep coadded images constructed from the individual scans serve as references for image subtraction, enabling a more sensitive search of new transient events (the template is essentially noiseless in the detection process). Finally, the deep coadds also allow identification of faint host galaxies that are otherwise undetected in the single-scan images, which are frequently useful for prioritizing follow-up observations. The stripe contains over 3 million cataloged galaxies that are brighter than $r \sim 22.5$ mag.

Due to gaps between the six CCD columns, the SDSS imaging camera is capable of scanning approximately half of the stripe (or one strip) in a single night. During the 2005

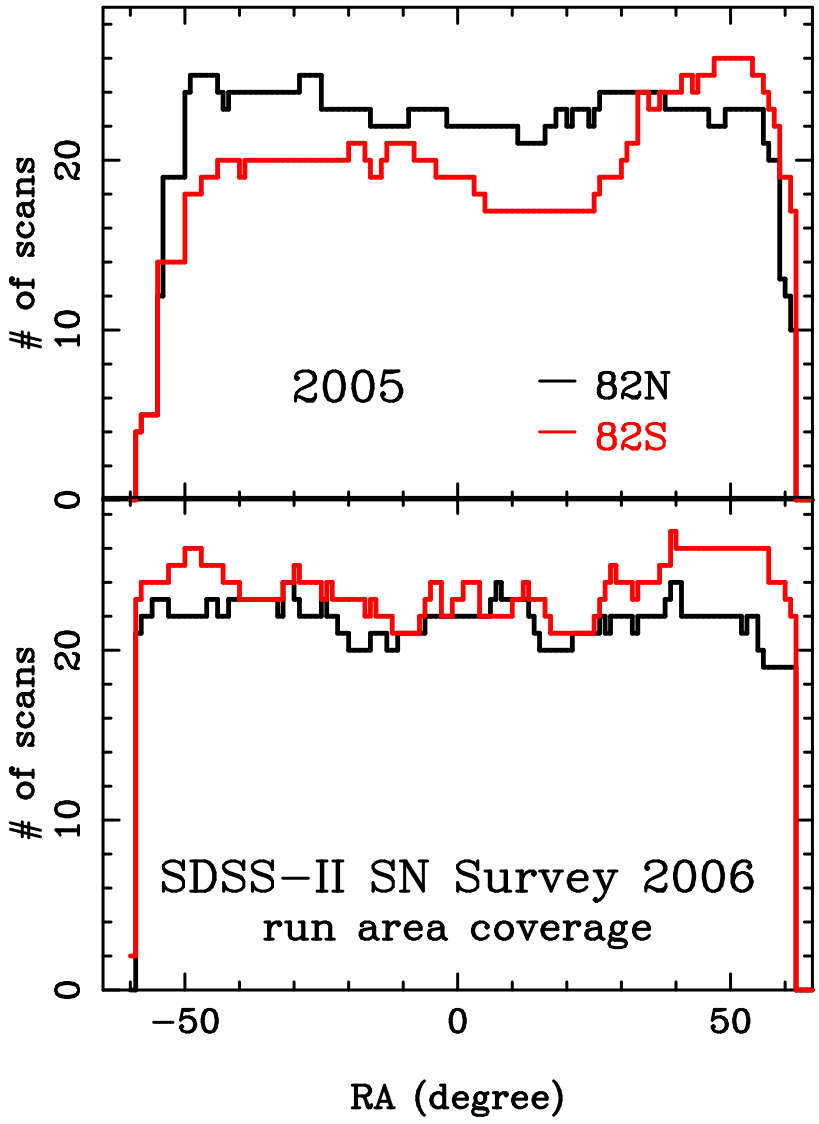

Fig. 1.— Number of imaging scans of the northern (black) and southern (red) strips for the 2005 (top) and 2006 (bottom) seasons as a function of right ascension. Note that, in contrast to the 2005 season, the 2006 scans are more evenly distributed in right ascension with very little difference between the northern and southern strips.

season, the observations alternated between the northern strip (82N) and the southern strip (82S) from night to night. In 2006, however, a significant effort was made to avoid long temporal gaps in any given part of the strip, so pieces of RA ranges from both strips were sometimes observed in a single night. We also note that approximately 10% of Stripe 82 is covered by both the northern and southern strips due to overlapping CCD columns, so

~ 30 deg^2 of the sky is observed on a cadence of 1 day (modulo weather losses). The lists of all SDSS-II SN runs, i.e., continuous imaging scans, and their corresponding RA ranges taken during the 2005 and 2006 seasons are given in Table 2 and Table 3, respectively. We also show in Figure 1 the number of visits made to each of the strips in 2005 and 2006 as a function of the RA. The complete set of corrected frames and the uncalibrated object catalogs from 2005 and 2006 are available online as part of the first SN data release (DRSN1[7]). These data are also accessible from the Data Archive Server of the Sixth Data Release[8] (Adelman-McCarthy et al. 2007).

2.2. On-Mountain Processing

The SDSS 2.5m telescope nominally performs observations every night during the search seasons, so the data must be processed within 24 hours to avoid a backlog of unprocessed data and to rapidly identify SN candidates for spectroscopic follow-up observations. A single night of observing produces up to $\sim$ 200 Gb of imaging data, so it is highly desirable to process the data on the mountain and significantly reduce the number of images that are transferred over the internet for visual inspection.

The data are processed on a dedicated 10 dual-processor (20 processors total) computer cluster that runs at APO. There are nine computers that process data; each of the 18 processors is responsible for processing all images from a single combination of filter (*gri*) and camera column (1 – 6). Each computer has 400 Gb of RAID5 disk and 2 Gb memory. The 10th monitor/backup computer has 3 Tb of disk and 4 Gb memory and is used for process-management, data transfer, and software development. This setup was specifically chosen to meet our requirement of processing a full night's worth of data within 24 hours. An 11th computer is available as a spare but so far has not been needed – during the first two years of operation, there were no serious failures. Several disks failed, but the RAID system worked properly to prevent any loss of processing time while waiting for a disk to be replaced. There was one curious glitch that may be related to operation at high altitude (2800 m). On occasion one of the computers would hang up, and cycling the power was the only way to revive the system. There were about 20 such incidents per season, although the probability seemed higher in the month of November, possibly due to better weather and longer nights resulting in more computing time. Since people are present at APO day and night, minimal processing time was lost from these hang-ups.

---

[7]http://www.sdss.org/drsn1/DRSN1_data_release.html

[8]http://www.sdss.org/dr6/access/index.html

There are three main tasks for the process manager: (i) start jobs, (ii) monitor processing progress, and (iii) monitor disk space. Due to the structure of the data acquisition system, the image processing can start only after an imaging run has finished, and the master script is usually executed manually by a person in the morning. While this script could have been automatically started, it is better that a human reviews the observer logs and checks that processing starts smoothly. The master script schedules and allocates resources for copying data from the data acquisition computer to a local disk, photometric reduction in *ugriz* (§ 2.2.1), and frame subtraction (§ 2.2.2) and object detection (§ 2.2.3) in *gri*. Several monitor scripts are used to check the status throughout the $\sim$ 20 hours needed to process the data. Since data processing continues virtually round-the-clock, a few people often shared the monitoring burden. Continuous monitoring was necessary because there were two common problems that could interupt the processing. First, poor observing conditions caused the photometric reduction software to abort. In this case, the photometric reduction must be reprocessed with a more restrictive RA range. The second source of interruption was the computer hang-ups discussed above. The last process-manager issue concerns disk space. Rather than clearing disk space after each night's data have been processed, we kept all of the subtracted images at APO for 1–2 weeks. The reason for keeping subtracted images is that for interesting candidates we could go back to earlier epochs and process u and z: u band was particularly useful to distinguish Type Ia and Type II supernovae. In addition, since the candidate position is known, we re-ran *gri* photometry at the known location in previous epochs to get a better estimate of the early-epoch fluxes and upper limits. The disk space was managed with a priority system so that clearing disk was mostly based on following a pre-defined algorithm and rarely involved a hasty decision. To avoid risks with automated disk-cleaning, a human-entered command was required.

Below we describe the search pipeline and the reduction procedures adopted to take the raw images to the point where they are transferred to the central SN database server at Fermilab.

2.2.1. PHOTO

The raw data are first processed through the `Photo` pipeline (Lupton et al. 2001, 2002; Stoughton et al. 2002). The software produces the corrected frames and generates bad-pixel maps, position-dependent PSF, and astrometric solution (Pier et al. 2003) that are used in subsequent processing stages. Our version of `Photo` does not identify sources in the images or perform photometric measurements (Hogg et al. 2001; Smith et al. 2002; Ivezić et al. 2004; Tucker et al. 2006), as they are not appropriate for efficiently identifying SN candidates,

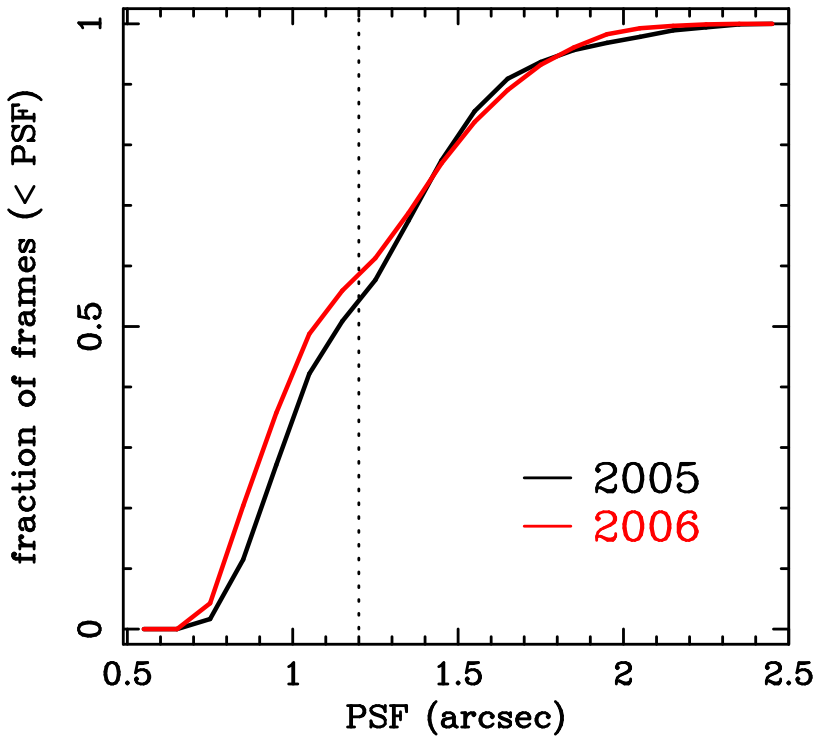

Fig. 2.— Cumulative distributions of the r-band PSF during the 2005 (black) and 2006 (red) search seasons. More than half of the frames were acquired at $< 1.2''$. Only frames successfully processed through `Photo` are included.

which are usually blended with their host galaxies. As with all standard SDSS data, images from each camera column are written in frames of 2048×1361 unique pixels or $13.51' \times 8.98'$ on the sky. The pipeline software was slightly tweaked to run on data taken under poor observing conditions (bright moon, low atmospheric transparency, and poor seeing). In 2005 and 2006, approximately 34% and 30%, respectively, of the frames were acquired when the moon was above the horizon. Figure 2 shows the distributions of the r-band PSF of frames successfully processed through `Photo` during the first two seasons.

2.2.2. Image Subtraction

To identify new transients in the search data, the images are run through a difference imaging pipeline, which matches the PSF of the search and template frames, adjusts for the difference in photometric zeropoint, accurately registers their pixels, and performs the subtraction. The image templates were divided into four separate RA ranges so that human

scanning and target selection could begin well before the entire night of data was finished processing. The subtracted frames in each filter are searched for positive fluctuations that consist of at least 2 contiguous pixels each above 3.0 σ of the noise. The software is derived from version 7.1 of the `Photpipe` software used by the SuperMACHO and ESSENCE collaborations (Smith et al. 2002). Extensive changes have been implemented to operate successfully on processed SDSS data. The modified application is called `Framesub`.

The pipeline is operated in three modes: 1) `sdssred` mode, where the input of images is prepared for difference imaging. 2) `sdssdiff`, which performs a difference imaging analysis of the search data compared to the template data. To conserve computing time, only the *gri* frames are differenced and used for object detection. This is the default mode that produces the objects for manual inspection, and subsequently the SN candidates described below. 3) `sdssforce` mode, in which, after reliable detection of a supernova candidate, we difference *all* data on the object, including the u and z bands, and perform forced-positional photometry at the location of the candidate. The measurements of magnitudes by `sdssdiff` and `sdssforce` are referred to as *search* and *forced* photometry. The overall structure of the software and detailed descriptions of each mode are provided in Appendix A.

2.2.3. Object Detection and Filtering Algorithm

The individual peaks found by `Framesub` are filtered through a software called `doObjects` to remove statistical fluctuations and identify true astronomical sources. First, the single-filter peaks are matched by position to identify sources that are detected in at least two of the three *gri* filters within $0.8''$. These sources are flagged as *objects*. Significant negative fluctuations are not flagged. The list of objects is compared against the list of known variable sources (the veto catalog) constructed from previous scans of Stripe 82. Any object that matches the position of a known variable is filtered out. Most of the sources in this catalog are variable stars, active galactic nuclei (AGN), and other persistently varying sources. Approximately 10% (20%) of the objects identified by `doObjects` in 2005 (2006) were associated with sources in the veto catalog.

Given the large area covered by the survey and the overlap of the central RA range of Stripe 82 with the ecliptic plane, our detections are overwhelmingly dominated by solar system objects. The challenge is to remove as many of these objects as possible prior to handscanning, without filtering out real SN candidates. Objects with proper motions in excess of $\sim 1''$ per minute are easily rejected by requiring that the object is detected in the r and i bands within $0.8''$ (the filters are imaged in the order *riuzg* and the effective time difference between adjacent filters is 71.7 seconds). Objects that move as slowly as $\sim 0.2''$

per minute can be identified through motion between the g and r bands. Objects that move at a slower rate are slightly more difficult to identify; when they pass in front of a background galaxy, they can look like perfectly good SN candidates. Approximately 35% (40%) of the objects found in 2005 (2006) were tagged as moving objects and removed prior to human evaluation.

New transient sources are entered into a dedicated `MySQL` database and the cutout images are transferred to Fermilab for visual inspection.

2.3. Handscanning, Autoscanning, and SN Candidate Selection

In addition to epochs of SN light-curves, the difference imaging and object detection algorithms described above result in the detection of many background sources of variation, both physical and non-physical. In order to robustly reject background and allow us to focus further analysis on promising SN candidates, we require that a human visually inspect images of the objects, a process which we refer to as *handscanning*.

In addition to moving solar system objects, other major sources of contamination include artifacts caused by (1) subtraction of slightly misaligned images, which creates shapes with clusters of positive and negative counts (objects that we call dipoles) in the differenced images, (2) diffraction spikes, and (3) bright saturated stars. Satellite trails that are not properly masked by the software also contribute to the background. A small fraction of the dipoles are high proper-motion stars that have drifted between the epochs of the template and search images. Many of these background objects, however, can be quickly rejected by visual inspection. In Figure 3, we show a gallery of cutout search, template, and differenced images of various types of objects evaluated by scanners – none, artifact, dipole, variable, transient, SN gold, SN bronze, and SN other. All images shown are from the r band. In Figure 4, we show *gri* images of a moving object correctly flagged by the software. These images show the source moved between the g and r exposures, which are separated by about 5 minutes.

As a convenient way for humans to handscan the detected objects, a web interface was constructed that queries the database and displays all of the relevant information about the object, including *gri* cutout images of the search, template, and differenced images, measured magnitudes, the mean sky coordinates and the relative positions measured in each filter, and a list of all previous detections (if any) within $0.8''$ of the object under inspection. The scanner evaluates the information and decides to either tag the object as a possible SN or to reject it as background. If an object is tagged as a SN and there are no previous detections

of objects within 0.8″, it becomes a new SN *candidate* with a unique SN ID number. A candidate will always remain a candidate unless it is manually vetoed by one of the scanners (which rarely occurs). All of the candidates can be accessed through a public web site[9].

During the 2005 observing season, we required that every object that is not rejected by `doObjects` be handscanned by a human. An average of about 3000 – 5000 objects were inspected per full night of imaging during the Fall 2005 season. Six scanners were on duty on a given night, each scanner responsible for inspecting all objects from one of the six camera columns, or 500 – 800 objects. Based on our experience in 2005, we made a number of changes to the handscanning procedure for the 2006 season described below.

2.3.1. Autoscanner

To reduce the number of objects to be scanned by humans, prior to the 2006 season we implemented a new software filter, called the *autoscanner*. The software performs two primary tasks: 1) identifies all objects detected in more than one epoch as well as bright (g or $r < 21$ mag) objects detected for the first time, and 2) uses statistical classification techniques to identify and filter out first-epoch background non-SN objects.

The reasons for performing 1) are as follows. First, the selection of objects detected in more than one epoch provides a very robust way of eliminating moving objects, one of the major contaminants of the 2005 SN candidates. Second, the selection of bright first-epoch objects enables us to discover nearby SNe; we can thereby obtain spectroscopic observations well before maximum light and provide rapid alerts to the SN community. In addition, bright, single-epoch candidates provide a back-up list of spectroscopic targets for nights when the spectroscopy queue is not filled by promising multi-epoch candidates. Although most of our targets were spectroscopically observed after two or more epochs of photometry, in a few instances, we did obtain spectroscopic observations of SN candidates based on a single epoch of detection. In the selection of these objects, the autoscanner also identifies objects associated with either a known variable in the veto catalog or a known SN candidate. In the former case, the object is filtered out. In the latter case, since there is no need for a human to scan the object, it is instead flagged by the autoscanner as a known SN candidate, stored in the database, and used in the light curve analysis (see Section 3.1).

For 2), the autoscanner attempts to identify and filter out bright first-epoch objects that belong to one of three classes of background; unmasked diffraction spikes, artifacts

[9]http://sdssdp47.fnal.gov/sdsssn/candidates/candTable.php

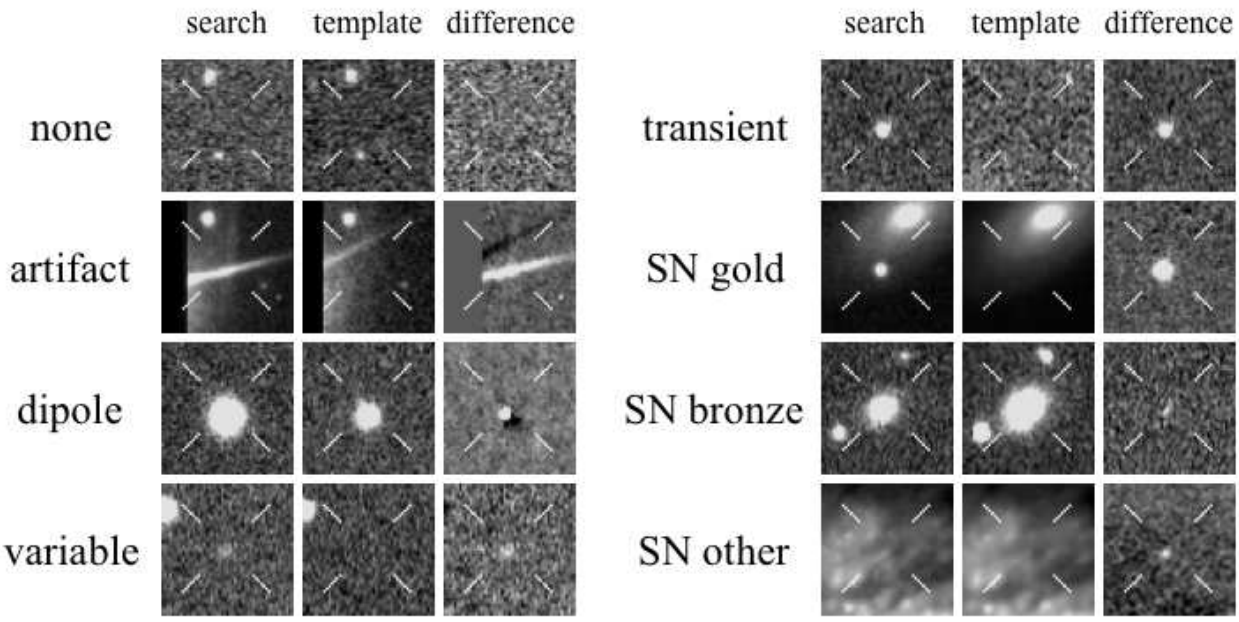

Fig. 3.— A gallery of various types of objects that a scanner evaluates. The panels show r-band search (left columns in each panel), template (central columns), and differenced (right columns) images of objects classified by scanners as "none", "artifact", "dipole", "variable", "transient", "SN gold", "SN bronze", and "SN other". Objects classified as "none" are typically detections near the threshold, and are often not visible to the human eye. Most "artifacts" are caused by different orientations of diffraction spikes in the search and template images. A "dipole" results from imperfect image registration as well as high proper-motion stars. A "variable" is an object associated with a persistent source and usually exhibits random temporal variability. These sources are newly variable sources that are not part of the veto catalog. A "transient" object is usually seen for the first time and *not* associated with a galaxy. The source can be a true SN with an undetected host galaxy or a slow-moving asteroid. An "SN gold" is a good SN candidate that is well-separated from the host. An "SN bronze" is a possible SN that lies close to the core of the galaxy and can, therefore, also be a variable active galactic nucleus. An "SN other" is also a possible SN, but is most likely a different type of variable source – in the case shown above, the source is a variable star in NGC1068 (M77). There is another category called "SN silver" (not shown), which is used for objects that are similar to a "transient", but detected in more than a single epoch (e.g., an SN with an undetected host galaxy). The distinction between gold/silver/bronze/other SN candidates is not important; all objects tagged as an "SN" become a SN candidate. Each cutout image is $20''$ on the side.

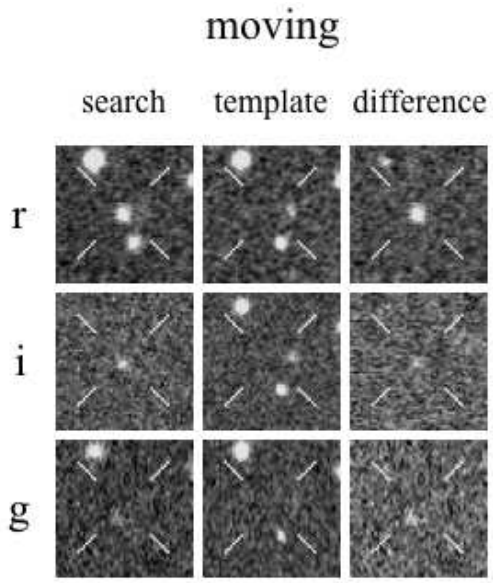

Fig. 4.— An example of a moving object that was correctly flagged by the autoscanner. As in Figure 3, the search, template, and differenced images are shown in the left, middle, and right columns, respectively. In addition to the r-band images (top row), we also display the g (middle row) and i-band (bottom row) images to show the relative position of the source in each filter. Note that the faint source in the g-band differenced image appears slightly below and to the left of the center of the image. The images are acquired in the order $ri(uz)g$ with a 71.7-second delay between each filter.

of imperfect image registration (dipoles), and moving objects. The software treats the set of objects, along with their evaluations by a human, from the 2005 search as a training set, and compares the observed quantities for newly detected objects against this set. The method used to classify an object is the *histogram method of probability density function (PDF) estimation*. In this method the observable quantities, or attributes, of an object form a multi-dimensional space, and a classification decision is made by considering the number count of objects, in the training set, from each class in a bin centered at the point describing the object we wish to classify. This method has the advantages of being non-parametric, allowing the decision boundaries in the observable space to be arbitrarily complicated, and of explicitly retaining the correlations between observables. A caveat of using the histogram method of PDF estimation is that one must have a sufficient number of objects in the training set to sample the PDF well in all regions of interest. With $\approx 90,000$ objects in the training set, this is not a significant limitation for the SDSS-II SN Survey. A technical discussion of the algorithm is presented in Appendix B.

During the 2006 observing season, the autoscanner was used to reject moving objects from among the set of bright first-epoch objects that were to be handscanned. For such bright objects, only $\approx 0.7\%$ of them are incorrectly tagged as moving objects by the autoscanner. In contrast to the 2005 observing season, we chose not to handscan epochs of known candidates or objects that showed variation in more than one observing season, and the autoscanner was used to reject such objects. Although some objects were classified as artifacts or dipoles, we chose not to reject these from the handscanning as they are a small fraction of the background in comparison to moving objects, and the relatively small reduction in handscanning that would be accomplished was determined to be outweighed by the risk of missing an early epoch of a nearby SN.

This new handscanning strategy and the autoscanner enabled a reduction in the number of objects scanned by more than an order of magnitude between 2005 and 2006, with no reduction in the quality or quantity of confirmed SNe. While scanning a single camera column in 2005 typically took $2-3$ hours per person for a full night of data, in 2006 a scanner could cover two columns in only $10-20$ minutes. The reduction of the 2006 handscanning by the autoscanner is summarized in Table 4.

A comparison of the objects classified by the autoscanner as artifacts to their human classification shows that the autoscanner is extremely efficient at recognizing artifacts, and that our concern about potentially rejecting nearby SNe was overly cautious. During the 2006 observing campaign, 3753 objects had been classified by the autoscanner as artifacts. Humans classified 2668 of these objects as artifacts and 3710 of them as some type of non-SN background. Of the remaining 43 objects classified by a humans as SN candidates, 41 were background (non-SN) erroneously classified by the scanner, one was a bright nova outburst, and one was the first epoch of a SN that was later (after the 2nd epoch detection) classified as a SN. Therefore, in cases where they disagree on classification of artifacts, the autoscanner appears to be more reliable than the human scanners.

3. Spectroscopic Target Selection and Follow-up Observations

Spectroscopic follow-up is an essential component of any current supernova survey, for both confirming the type of the SN candidate and measuring the cosmological redshift (preferably from host galaxy emission/absorption lines). For the SDSS-II SN survey, the amount of scheduled spectroscopic telescope time is larger than the amount of imaging time on the SDSS 2.5m telescope by a large factor (see also Frieman et al. 2007). The telescopes used for spectroscopy in 2005 and 2006 included the 9.2m HET, 3.6m NTT, 3.5m ARC, 8.2m Subaru, 2.4m MDM Hiltner, 4.2m WHT, 4m KPNO Mayall, 10m Keck, 2.5m NOT, and the 11m

SALT.

On any given night during the fall season, there could be several telescopes that are simultaneously scheduled and observing a set of our SN candidates. This requires a significant amount of coordination between the various observers at each of the telescopes to avoid observing the same candidate. A single person (the first author of this paper) was responsible for coordinating all follow-up imaging and spectroscopic observations in 2005 and 2006. Telescopes separated by several time zones are relatively easy to coordinate, but those that have similar longitudes (e.g., MDM, ARC, KPNO) require real-time communication. In general, the brighter targets are parsed to telescopes with smaller aperture, but the magnitude limits must be adjusted depending on the observing conditions at each site. We have made every effort to avoid taking duplicate spectra, but on occasion the same object was observed nearly simultaneously on two telescopes.

A good night of imaging of half of Stripe 82 typically yields $100 - 300$ objects that are tagged as *new* SN candidates, which are publicly accessible through the web[10] immediately after they are entered into the database. This number significantly exceeds the number of targets we can observe spectroscopically, and choices must be made. The following subsections describe the further prioritization of SN targets for spectroscopic observations. The algorithm and strategy depends on the amount of resources available, which is something that evolved quite substantially between the 2005 and 2006 search seasons.

3.1. SN Photometric Typing

After each night of imaging on the SDSS 2.5m telescope, the *gri* light curves of all active candidates are compared against a library of light curve templates of different SN types. The purpose of this procedure is twofold – 1) to quickly identify the best-matching template and provide estimates of the redshift, extinction, the approximate date of maximum light, and current apparent magnitudes, and 2) to compute other quantities that are useful for prioritizing follow-up spectroscopy, such as the amount of host galaxy contamination. The process is essential since the number of active SN candidates (a good fraction of which are not SNe) at any given time exceeds the number that can be observed spectroscopically by a large factor. A reliable system is necessary to make efficient use of the valuable spectroscopic resources. Several techniques and algorithms for SN photometric identification have been introduced previously by Poznanski et al. (2002, 2006), Johnson & Crotts (2006), Riess et al. (2004b), Sullivan et al. (2006), Kunz et al. (2007), and Kuznetsova & Connolly (2007). The

[10]http://sdssdp47.fnal.gov/sdsssn/candidates/candTable.php

method adopted here is most similar to that used by the SNLS spectroscopic follow up described in Sullivan et al. (2006). Below, we describe the details of the algorithm.

The measured light curves are compared against a library of light curve templates, which are grouped into three types – SN Ia, SN Ib/c, and SN II– and are generated from multi-epoch spectra constructed and compiled by P. Nugent[11] and also from the SUSPECT database[12]. Specifically, for the Type Ia, we use Nugent's Branch-normal, 1991T-like, and 1991bg-like templates. The Branch-normal spectra are used for computing synthetic light curves of SNe Ia with a range of luminosities parameterized by the decline rate. The model is described in Appendix C. The set of templates used for the Type Ib/c are Nugent's normal and hypernova Ib/c spectra, as well as spectra and light curves of SN1999ex and SN2002ap from the SUSPECT database. Similarly, we use Nugent's II-P, II-L, and IIn spectra, and SUSPECT's 1993J (IIb), 1998S (IIn), and SN1999em (II-P) to generate a set of Type II light curves.

The light curves in the observed *ugriz* filters are calculated on a grid of four parameters (z, A_V, $T_{\rm max}$, [$\Delta m_{15}(B)$, template SN]), where z is the redshift, A_V is the host galaxy extinction in the V band and assumes $R_V = 3.1$, and $T_{\rm max}$ is the time of rest-frame B-band maximum light. The last parameter refers to either the decline rate parameter for the Branch-normal Ia models ($\Delta m_{15}(B)$), or the particular SN template for the peculiar SNe Ia (1991T-like and 1991bg-like) and the core-collapse models. We do not attempt to fit or correct for the Milky Way extinction. In this procedure, we *assume* a cosmology to convert the redshift to a luminosity distance, similar to the method adopted by the SNLS described in Sullivan et al. (2006). The adopted cosmological parameters are $\Omega_m = 0.3$ and $\Omega_\Lambda = 0.7$. For the SN Ia templates, we also assume a fiducial peak B-band absolute magnitude of $M_B = -19.0 + 5\log(H_0/70)$ mag, where H_0 is the Hubble constant in units of km/s/Mpc, for a standard $\Delta m_{15}(B)$= 1.1 SN Ia. As shown by Sullivan et al. (2006), a particular set of assumed cosmological parameters in the computation of the model light curves does not significantly bias the population of targets for spectroscopic observations. At low redshift ($z \lesssim 0.2$), the luminosity distances are not sensitive to our choice of Ω_m and Ω_Λ. Above $z \sim 0.2$, the statistical uncertainties in the fluxes and the combination of varying z and A_V can compensate for differences in luminosity distance that might result from a different set of cosmological parameters. The assumption, however, could systematically bias the estimated photometric redshifts, but that is not a concern for the purposes of target selection.

The templates are grouped into three SN types – Ia, Ibc, and II – and the fitter records

[11]http://supernova.lbl.gov/ nugent/nugent_templates.html

[12]http://bruford.nhn.ou.edu/ suspect/index1.html

the best-fit parameters and the minimum value of the χ^2 statistic on the four-dimensional parameter grid within each of the three types. In addition to identifying the SN type with the lowest χ^2 value, which we refer to as "type-best", we examine the relative values of the χ^2 and determine whether the SN candidate should be considered as "typed" according to one or both of the following two criteria. If we denote the value of the χ^2 of the best-matching type by $\chi^2_{\rm min}$, the next best type as χ^2_1, and the worst one as χ^2_2 (i.e., $\chi^2_{\rm min} < \chi^2_1 < \chi^2_2$), the "A" criterion is satisfied if $\chi^2_{\rm min} < \chi^2_1 - \chi^2_{\rm min}$. If "type-best" is a Ia *and* satisfies the above criterion, the candidate is said to have a "type-A of Ia". The "B" criterion is satisfied if $\chi^2_{\rm min} < N(\chi^2_{\rm min} + \chi^2_1 + \chi^2_2)/3$ with $N = 0.5$. Similarly, if the best-fit type is a SN Ia and satisfies the above χ^2 criterion, the candidate is said to have a "type-B of Ia". The value of 0.5 adopted for N works well for SN candidates with low S/N, and was empirically determined from a sample of spectroscopically confirmed SNe from our 2004 engineering run (Sako et al. 2005). Also computed are the estimated current g and r magnitudes from the model light curves. We also search for the nearest galaxy within $10''$ from the SN position in the SDSS galaxy catalog and refit and retype the light curves using the best estimate of its redshift as a prior. We adopt galaxy photometric redshifts from Oyaizu et al. (2007) and spectroscopic redshifts from the SDSS DR5 (Adelman-McCarthy et al. 2007).

We note that the absolute χ^2 values for the model fits do not appear to be very meaningful. The models have not been calibrated against real data and there are no errors associated with the light curves (see, e.g., Appendix C). The current implementation also does not attempt to reject outlier points due to poor zeropointing and imperfect image registration, which are common features of the search photometry. The best-fit χ^2 value for the SN Ia model of a true SN Ia may be large compared to the number of degrees of freedom, but the confidence can be high if that value is well below the values of the other SN types. The *relative* values of the χ^2 are, therefore, important and useful discriminators. In Figure 5, we show the values of $\chi^2_{\rm min}$, $\chi^2_1 < \chi^2_2$, and 0.5 $(\chi^2_{\rm min} + \chi^2_1 + \chi^2_2)/3$ as functions of the number of epochs for SN2006fz, a Type Ia at z=0.105, with a flat galaxy photometric redshift prior. For this candidate, the model with the minimum χ^2 corresponds to the SN Ia model, and both the "A" and "B" criteria are satisfied at all epochs. Also shown in Figure 6 are the light curve fits to SN2006fz using the first 2, 4, 6, and 8 epochs of search photometry.

The overall performance of the photometric typing software is demonstrated in Figure 7, where we plot the fraction of the spectroscopically confirmed SNe Ia, whose best-fit model is that of a SN Ia as a function of the number of the light curve epochs. The figure also shows the fraction of SN Ia that satisfy one of the "A" or "B" criteria with or without a nearest-neighbor host galaxy redshift prior. Note that the fractions increase between 2 to ~ 4 epochs, but the improvement beyond ~ 5 epochs is marginal. The fraction with the best type equal to a Ia does not reach unity because the spectroscopic sample includes 1) peculiar SNe Ia,

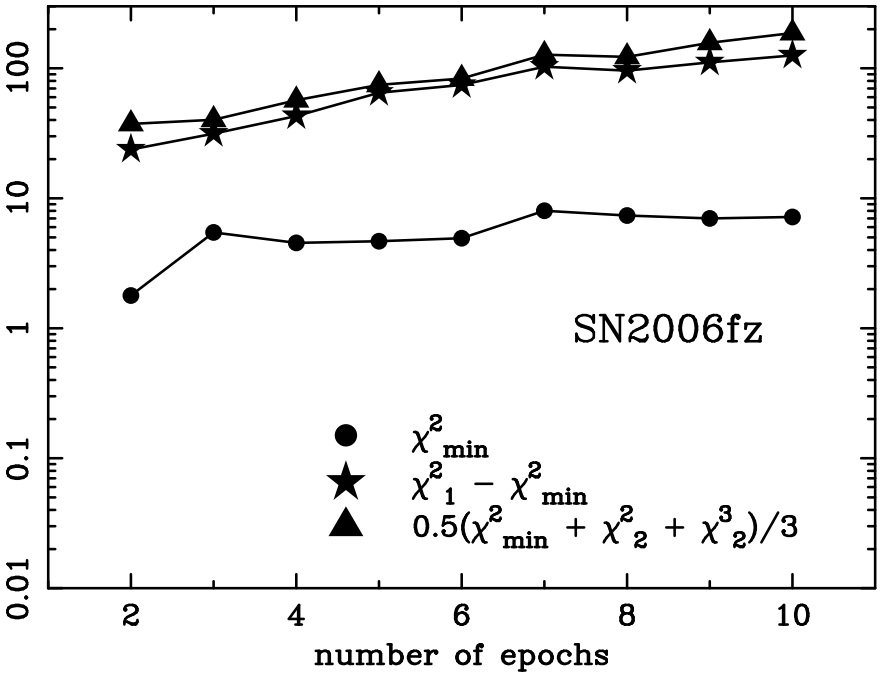

Fig. 5.— Fit results for SN2006fz (SN Ia at z=0.105; internal candidate ID 13135) as functions of the number of epochs in the light curve. The bottom curve (labeled with filled circles) shows the minimum χ^2 values, which at every epoch correspond to the Ia model. The top two curves labeled with filled stars and triangles show values relevant for the "A" and "B" typing criteria, respectively. For this particular SN, $\chi^2_{\rm min}$ is always below these two curves, which implies that this SN is a Type Ia at high-confidence.

2) candidates with poorly subtracted images and photometry epochs, 3) SNe Ia discovered well after maximum light, and 4) SNe with low-S/N light curves whose best-fit type drifts with the number of epochs. Candidates that fall into the first three categories were targeted for spectroscopy because they were nearby and bright enough to be observed on 3-m class telescopes, and those candidates were observed even if their best-fit photometric type was not a SN Ia (see § 3.3). The candidates in the fourth category were observed because they were at one time typed as a SN Ia. We also show in Figure 8 the time of B-band maximum light estimated from 2 – 4 light curve epochs in comparison with the "final" estimate of the peak using the full light curves. Again, the reliability improves substantially between 2 and ~ 4 epochs.

Studies of the software and handscanning efficiencies as functions of the object brightness with the fakes (see Section A.2) show that the SN candidate identification and spectroscopic follow-up observations are essentially complete out to $z \sim 0.12$ (Dilday et al. 2007). The one

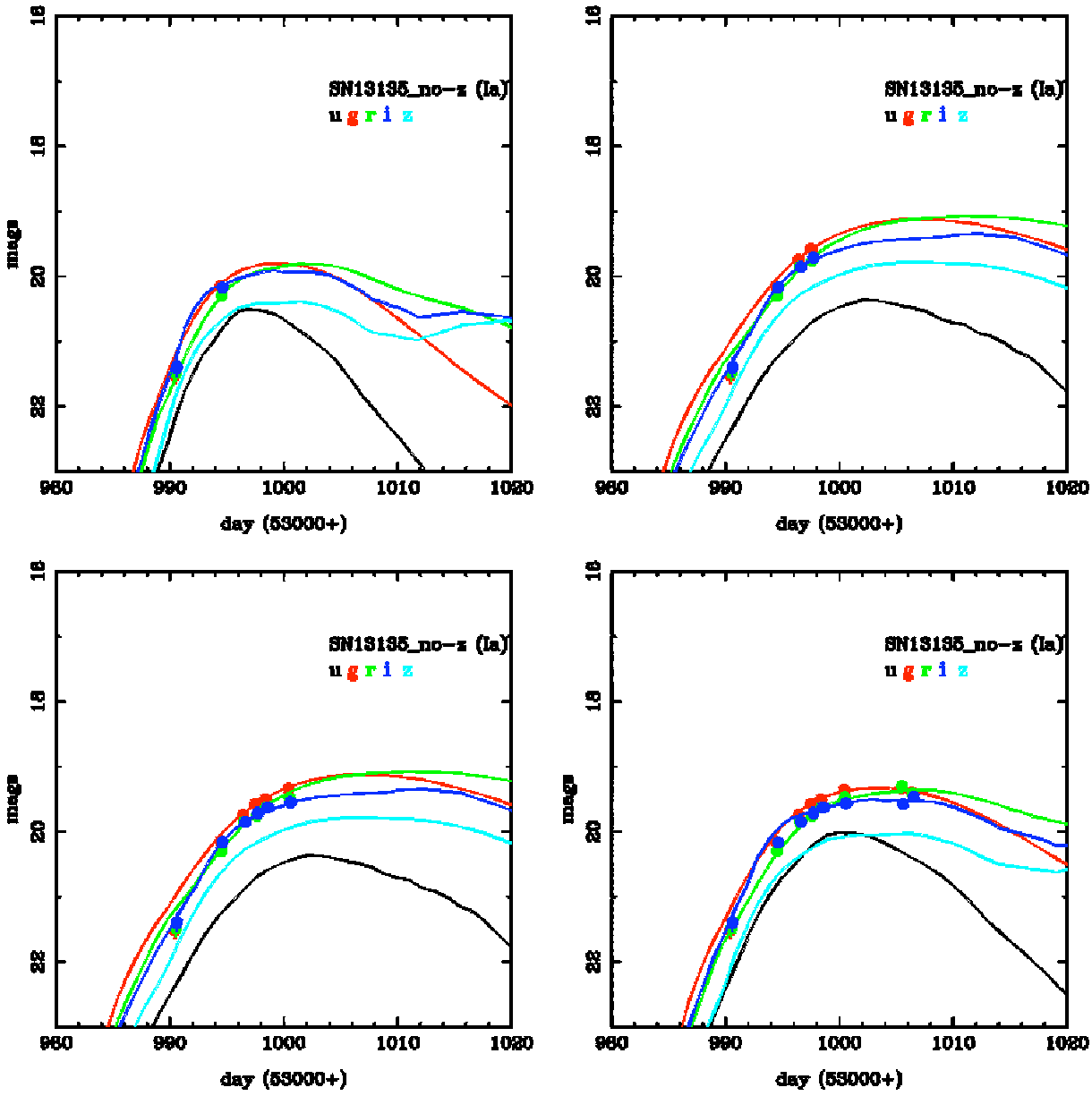

Fig. 6.— Light curves of SN2006fz (same SN as shown in Figure 5) and fits to the best-fit SN Ia models after 2, 4, 6, and 8 epochs of detections without a galaxy photometric redshift prior. Search photometry from *gri* are shown. Model light curves in u and z are shown as well.

exception to this is our bias against highly-extincted SNe, since the grid of light curve models did not extend beyond $A_V = 1.0$ in 2005 and $A_V = 3.0$ in 2006. A post-season analysis of

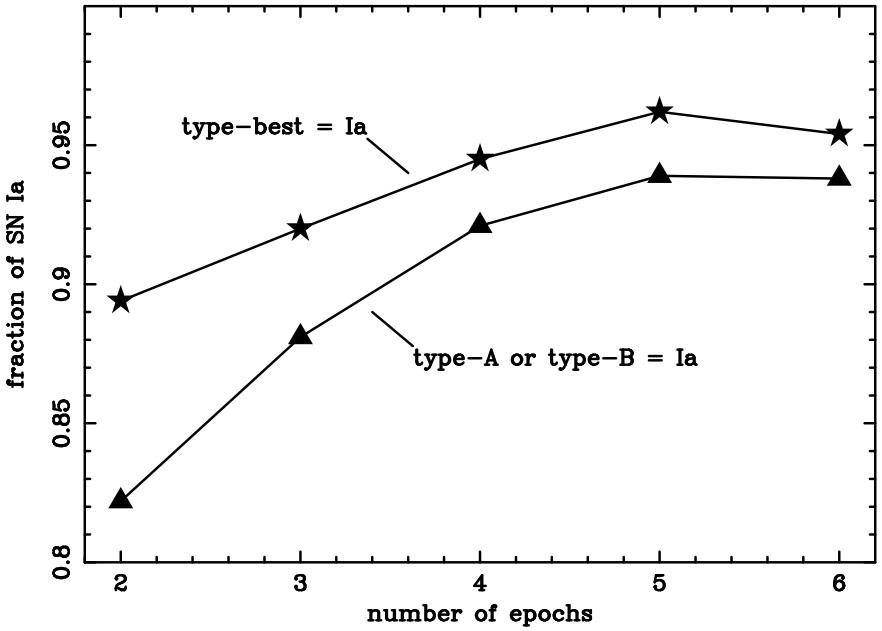

Fig. 7.— The fraction of spectroscopically confirmed SNe Ia whose best-fit model is that of a SN Ia as a function of the number epochs (top curve with stars). Also shown is the fraction of SNe Ia, which satisfy one of the "A" or "B" criteria with or without a galaxy redshift prior (bottom curve with triangles). A large fraction of the sources ($> 80\%$) are typed as SN Ia after only 2 epoch of imaging.

the 2005 candidates with an extended A_V range recovered two additional photometric SN Ia candidates with large extinction in this redshift range. There is no evidence for an additional population of low-z SNe Ia that were missed due to the models adopted.

The light curve fits generally run on the *gri* search photometry, which is usually accurate to within ~ 0.1 mag. Whenever the computer cluster at APO is idle, we run the pipeline in `sdssforce` mode (see, §2.2.2) to produce u and z-band differenced images from all runs available on the mountain for each of the SN candidates. This typically includes frames from several pre-discovery epochs. The u-band photometry is sometimes useful for distinguishing SNe Ia from core-collapse SNe that are generally bluer ($u - g \lesssim 0.5$) during the early phases after explosion.

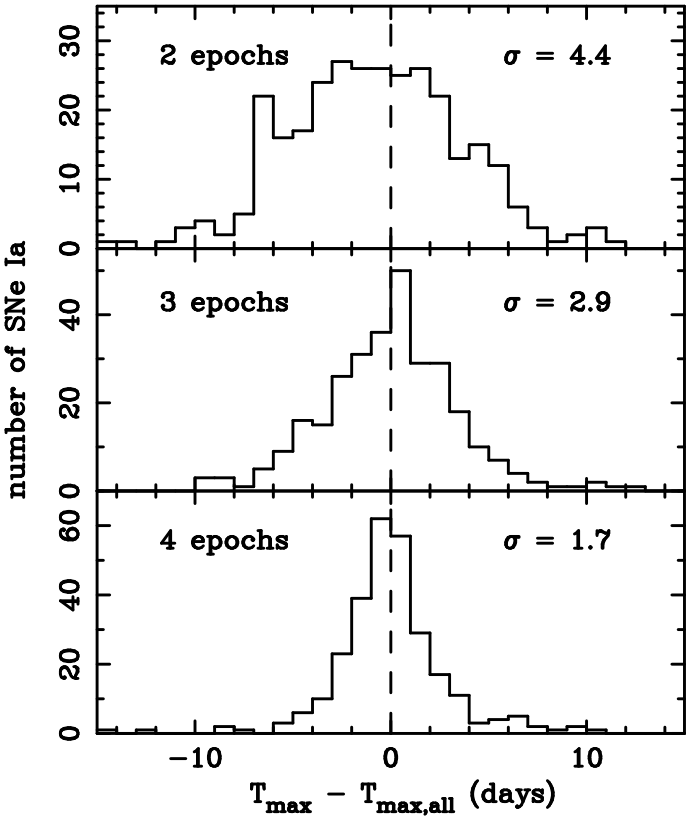

Fig. 8.— Distribution of the difference between the time of B-band maximum estimated using the full light curves and that using the first 2 (top), 3 (middle), and 4 (bottom) epochs of the spectroscopically confirmed SNe Ia. Values are taken from fits with a flat redshift prior. The distributions are fit with a single gaussian, and the σ values are listed in each panel. The width of the distribution stays approximately constant above 4 epochs. The vertical dashed lines represent the x-axis origin; not the centroid of the distributions.

3.2. Observability Index

After the SN photometric typing process, the software computes three quantities that help prioritize the target list for spectroscopic observations. These quantities are referred to as "weights" and they are constructed specifically to identify candidates that are 1) near or before peak brightness, 2) less contaminated by galaxy light, and 3) not heavily extincted by intervening dust. The product of the three weights defines the "observability index"; candidates with higher observability index are generally assigned higher priority.

For 1), we define the "time weight" as,

$$W_C = \begin{cases} e^{|t|\{\Delta m_{15}(B)/[10(1+z)]\}} & \text{if } t < 0 \text{ days;} \\ e^{-t\{\Delta m_{15}(B)/[20(1+z)]\}} & \text{if } t \geq 0 \text{ days,} \end{cases} \quad (1)$$

where t is the current estimate of the SN epoch in days relative to B-band maximum brightness. Note that W_C is large when the SN is young, as SN are most easily classified near maximum light (Filippenko 1997), and decays exponentially with a characteristic time scale of 20 days. The decline-rate parameter $\Delta m_{15}(B)$ and redshift z are also adopted from the best-fit values obtained from the light curve fits. If the best-fit type is a core-collapse SN, $\Delta m_{15}(B)$ is set to unity.

The second weight computed by the software is the "contamination weight" defined as,

$$W_T = e^{-2/\theta} \times \left(\frac{F_{\mathrm{SN},r}}{F_{\mathrm{Gal},r}} \right)^{1/2}, \quad (2)$$

where θ is the distance in arcseconds between the SN and the centroid of the nearest-neighbor host galaxy. The quantity $F_{\mathrm{SN},r}$ is proportional to the *current* r-band flux of the SN, again, as estimated from the best-fit light curve model,

$$F_{\mathrm{SN},r} = 10^{-0.4\ r_{\mathrm{SN}}} \quad (3)$$

and $F_{\mathrm{Gal},r}$ is the estimated local galaxy r-band flux at the position of the SN defined to be,

$$F_{\mathrm{Gal},r} = 10^{-0.4(r_{\mathrm{Gal}} + d/d_{\mathrm{eff}})}, \quad (4)$$

where d is the angular separation between the SN and the centroid of the nearest-neighbor source and d_{eff} is the effective radius of that source along position angle of the SN. This quantity is computed according to,

$$d_{\mathrm{eff}} = \frac{\mathtt{isoA}^2(1-e^2)}{1 - e^2 \cos^2 \phi}. \quad (5)$$

Here, ϕ is the position angle of the SN measured from the position angle of host galaxy's semimajor axis (`isoPhi`) with ellipticity given by,

$$e^2 = 1 - \left(\frac{\mathtt{isoB}}{\mathtt{isoA}} \right)^2. \quad (6)$$

The isophotal galaxy parameters (`isoA`, `isoB`, and `isoPhi`), which are used to measure the galaxy's ellipticity of the 25 magnitudes per arcsecond isophote, are adopted from the SDSS

DR4 catalog[13]. Clearly, candidates with larger values of W_T suffer less contamination from the host galaxy light.

The third and final weight is the "dust weight", which estimates the amount of dust extinction from both host galaxy morphology and color, and is defined to be,

$$W_D = e^{-d_{\rm eff}/d} \times (1 + 3\ f_{\rm deV} + 5\ c_{\rm ellip}), \tag{7}$$

The quantity $f_{\rm deV}$ is the fractional probability of the source being well represented by a de Vaucouleurs profile and is again computed from values in the SDSS catalog, i.e.,

$$f_{\rm deV} = \frac{\texttt{deV\_L}}{\texttt{deV\_L} + \texttt{exp\_L} + \texttt{star\_L}}, \tag{8}$$

where `deV_L`, `exp_L`, `star_L` are the null hypothesis probabilities of the object being well-represented by a de Vaucouleurs profile, an exponential function, and a stellar profile (PSF), respectively. The last quantity in parentheses of Equation 7 characterizes the color of the galaxy, and is defined to be,

$$c_{\rm ellip} = \begin{cases} (r_{\rm Gal} - i_{\rm Gal} - 0.4)/0.2 & \text{if } (r_{\rm Gal} - i_{\rm Gal}) > 0.4 \text{ and } (g_{\rm Gal} - r_{\rm Gal}) > 0.9; \\ 0 & \text{otherwise,} \end{cases} \tag{9}$$

where $g_{\rm Gal}, r_{\rm Gal}, i_{\rm Gal}$ are the host galaxy g, r, and i-band model magnitudes. This quantity is non-zero only for red elliptical galaxy candidates, which typically populate the color-color space bounded by $(r-i) > 0.4$ and $(g-r) > 0.9$. Note that the light curves also provide an independent (and usually more reliable) estimate of the amount of dust extinction.

The final observability index is defined as the product of the three weights,

$$\text{observability index} = W_C \times W_T \times W_D. \tag{10}$$

In practice, the observability index is rarely used for the bright ($r \lesssim 20.5$ mag) low-z SN candidates, since there are enough spectroscopic resources to observe nearly all of those targets. At high z, however, the number of SN Ia candidates exceeds the number we can observe given our limited resources on large-aperture telescopes. In order to select the best targets from a large number of candidates that satisfy the light curve selection criteria, the sources are ranked based on the value of the observability index. Manual screening and selection of the sources by the spectroscopic coordinator is still required. We describe our strategy in detail below.

[13]http://www.sdss.org/dr4/algorithms/classify.html

3.3. Spectroscopic Follow-up Strategy

Spectra are obtained by the various spectroscopic teams, who independently apply for observing time during each of the search seasons. The teams agreed to confirm types and obtain redshifts of SN Ia candidates at the highest priority, but each team generally has one or more of their own SN projects that they pursue in parallel. Some of these include 1) multi-epoch spectroscopy of peculiar SNe, 2) SNe in underluminous host galaxies, 3) SN Ib/c and hypernova candidates, 4) detailed spectroscopic properties of SN Ia hosts, and 5) multi-epoch studies of line features and their diversity in SNe Ia. Whenever possible, we also try to obtain spectra of other variable objects if a scanner has classified them as "interesting". An example of this is a dwarf nova discovered in Aquarius (Prieto et al. 2006).

In 2005, the primary telescopes used for observing the low-redshift candidates were the ARC 3.5m, WHT 4.2m and the MDM 2.4m telescopes. The high-z candidates were observed with either the HET or Subaru. The resources were sufficient to obtain spectra of most $z \lesssim 0.15$ SN Ia candidates as well as core-collapse SNe at $z \lesssim 0.06$, but only a fraction of the $z \gtrsim 0.15$ candidates were observed.

During the Fall 2006 campaign, the various spectroscopic teams were awarded sufficient 3m-class telescope time to obtain a spectrum of essentially *all* SN candidates with $r \lesssim 20.5$ mag (an average SN Ia at $z \lesssim 0.15$ and core-collapse SN at $z \lesssim 0.06$ near maximum light) *and* obtain multi-epoch spectra of a large sample of nearby ($z \lesssim 0.1$) SNe Ia.

We generally require at least two epochs of detection before we target the candidate for spectroscopic observation, to guarantee that the source is not an asteroid. This also enables a better estimate of the epoch of peak brightness of the SN. Since the primary goal of our survey is to obtain well-sampled light curves of Type Ia SNe, SN Ia candidates that are discovered early are generally given higher priority for spectroscopy. This is especially true for the very low-z candidates ($z \lesssim 0.1$) to enable rapid confirmation and dissemination to the public.

In practice, we initially select SN Ia candidates that satisfy at least one of the "A" or "B" criteria either with or without a galaxy photometric redshift prior. There are times, however, during stretches of poor weather at APO and/or when several 3m-class spectroscopic telescopes are online, when there are not enough new and bright SN Ia candidates to observe. This was not an issue during most of the 2005 season, but it occurred frequently in 2006. In such cases, we loosen the selection criteria and inspect all currently-bright sources irrespective of their best-fit SN type; there is only small number ($\sim 30-50$) of sources with $r \lesssim 20.5$ mag at any given time. When necessary, we also target candidates that have only a single epoch of detection. Extremely red single-epoch targets that are not associated with a host galaxy

are generally avoided (to minimize the chance of observing an asteroid).

On the other hand, there is never a shortage of higher-z SN Ia targets at $z \gtrsim 0.2$, so the "A" or "B" criterion with or without a galaxy photometric redshift prior is always used in the pre-selection process. At these redshifts, we generally avoid candidates that are located within $\sim 0.5''$ of the centroid of a host galaxy, since they have a relatively higher chance of being an active galactic nucleus. Candidates at $z \sim 0.3$ that are well-separated from the host and suffer a relatively low level of extinction (as estimated from the multi-band light curve fits) are high-priority (priority 0 and 1) targets for HET, which is a queue-scheduled telescope (Shetrone et al. 2007). Lower-z candidates ($z \sim 0.2$) are assigned lower HET priority (mostly priority 2, but some at priority 3). Targets are generally kept active in the HET queue until they are ~ 20 days past maximum light as estimated from the light curve fits. The Subaru telescope has focused on SN Ia candidates in a similar redshift range, but, to take advantage of its superb image quality, the Subaru telescope has generally been assigned targets that suffer a relatively large amount of host contamination (i.e., a low value of W_C; see Section 3.2).

The spectra are often analyzed in real time by the observers on site, and feedback is given to the spectroscopic coordinator. Depending on the observing conditions, the target list is adjusted in real time. At the end of the night, the observers provide a preliminary spectroscopic type of each of the candidates observed. The type and the preliminary redshift is entered immediately into the database, and the results are disseminated to the community through the Central Bureau Electronic Telegrams. All nearby SNe ($z \lesssim 0.08$), however, are also announced to a list of subscribers via email usually within hours from confirmation, allowing rapid complementary follow up on other telescopes. Information on all spectroscopically confirmed SNe is placed on a public web page[14] as soon as the SN type has been entered into the database. A list of all spectroscopically confirmed SNe from 2005 and 2006 is presented in Tables 5 and 6, respectively.

4. Imaging Follow-up

Throughout the 2005 search, we used some of our ARC 3.5m and MDM 2.4m time, as well as the imager on the NMSU 1m telescope, University of Hawaii 88-inch telescope, the 1.8m Vatican Advanced Technology Telescope (VATT), and the 3.5m WIYN telescope to (1) augment the light curve points of spectroscopically confirmed SNe Ia during periods of poor weather conditions at APO and (2) obtain late-time photometry of SNe that had

[14]http://sdssdp47.fnal.gov/sdsssn/snlist_confirmed.php

faded below the SDSS detection limit. Some imaging observations were performed by the VATT, the WIYN, and the 1.5m telescope at Maidanak Observatory during the 2006 season. Additional imaging data were obtained on the ARC 3.5m during November of 2006 when the Dual Imaging Spectrograph was not functional. This effort of follow-up imaging was not carried over for the MDM and for ARC during September and October, since we concluded that spectroscopy is the more valuable use of our resources. In December of both 2005 and 2006, however, imaging observations were performed to get light curves of SNe discovered in November past maximum light. Deep multi-band imaging of several host galaxies of SNe Ia were also obtained by the 2.5m Isaac Newton Telescope.

A few high-profile SDSS-II SN targets were also observed extensively by several follow-up programs – optical imaging and spectroscopy by the CfA SN Group, optical and infrared imaging and optical spectroscopy by the CSP, and optical spectroscopy by the SNFactory.

5. Results from Fall 2005 and 2006

The 2005 season resulted in 73 unique SDSS imaging runs acquired on 59 different nights. Approximately half of the frames were taken under non-photometric conditions, bright moon, and/or poor seeing. A total of 155,616 objects were visually inspected during this season, of which 24,402 were tagged as potential SNe, resulting in 11,385 unique SN candidates (see Table 7). Interestingly, 6,618 of those candidates were detected in only a single epoch, and are mostly likely moving solar system objects that were not filtered properly. A few of these single-epoch candidates may be fast transients that rise and fade on timescales shorter than ~ 1 day (Becker et al. 2004). Most of the remaining 4767 candidates are true variables or transient sources[15]. A short summary of the 2005 and 2006 seasons is shown in Table 7.

For the 2005 search season, we acquired 248 spectra from 187 distinct SN candidates under various observing conditions. A total of 130 unique candidates were spectroscopically confirmed to be of Type Ia. One of these SNe Ia (SN2005hj) was co-discovered and spectroscopically observed by the Texas Supernova Search (Quimby et al. 2007). The number of confirmed core-collapse SNe were 7 and 13 for Type Ib/c and II, respectively. One of these Type II SNe (SN2005mj) was spectroscopically confirmed by the ESSENCE Group. An additional 40 candidates were observed in the post-season during December 2005 – January 2006. A sample of 41 SN targets including SN2005hk (Phillips et al. 2007) and SN2005gj (Prieto et al. 2007) for which we acquired 16 and 9 spectra, respectively, were observed spec-

[15]A very small fraction of the 4767 multi-epoch candidates are artefacts of image subtraction – e.g., faint dipoles that appear in the same place at two or more different epochs.

troscopically more than once. The host galaxy of one 2005 candidate (SN7017) was observed during the 2006 search season. Interestingly, that supernova was still active and visible a year after discovery; the spectrum was identified as a peculiar SN similar to SN2002ic and SN2005gj.

In 2006, 90 SDSS imaging runs were taken on 60 nights. The number of visually-inspected objects was reduced by more than an order of magnitude to 14,430. This improvement is due to the modified moving object finder and the choice of scanning only second-epoch and bright first-epoch objects. We identified a total of 3694 unique SN candidates. Surprisingly, there is still a somewhat large sample (599 out of 3694) of slow-moving single-epoch objects that were tagged by a scanner as a possible SN and made the candidates list.

During the second search season, a total of 449 spectra were acquired, $\sim 80\%$ more than the 2005 season, from 285 unique candidates. Though the majority of these were observations of new 2006 candidates, a handful of host galaxies of the 2005 candidates were observed as well. A sample of 197 candidates, including five candidates that were observed by the CfA SN Group and the ESSENCE Survey, were spectroscopically confirmed to be SNe Ia and 14 candidates were identified as spectroscopically probable SNe Ia. The number of confirmed core-collapse SNe were 7 and 19 for Type Ib/c and II, respectively.

Table 8 summarizes the spectroscopic observations grouped into candidates discovered in 2005 and 2006. We performed 172 (241) observations of new SN Ia candidates discovered in 2005 (2006), of which 130 (197) were spectroscopically confirmed to be SNe Ia, and 16 (14) candidates were identified as spectroscopically probable SNe Ia; the latter are denoted SN Ia? in Tables 5 and 6. In addition, observations of 7 (7) additional candidates in 2005 (2006) resulted in galaxy spectra (either the SN had faded or the galaxy was too bright relative to the SN) with spectroscopic redshifts consistent with photometric redshifts estimated from the multi-band light curves of the SNe. Therefore, in the first two years, 90% of SN Ia targets resulted in spectra of SNe Ia, probable SNe Ia, or host galaxies of photometric SN Ia candidates. A total of 12 SN Ia targets (3%) were classified instead as core-collapse SNe, 4 targets (1%) were classified as either an AGN or a flaring M-dwarf, and 9 targets (2%) resulted in galaxy spectra with spectroscopic redshifts inconsistent with photometric redshifts estimated from the SN Ia model fits. Finally, there is a sample of 18 spectra (4%), most of which were taken under poor weather conditions, that are unidentified.

Evaluation of the full light curves after the end of each search season enables identification of additional photometric SN Ia candidates that, for various reasons, were not spectroscopically observed during the search. We have identified at least ~ 200 high-quality SN Ia candidates from the 2005 candidates list, and have already acquired host galaxy spec-

tra for a significantly-sized subsample. These targets are also good fillers during periods of poor observing conditions at APO that result in a lack of good new SN candidates. As of the writing of this paper, we have measured redshifts for 81 host galaxies of candidates with Ia-like light curves. An additional 13 candidates were identified to be good Ia candidates with host galaxy redshifts from the SDSS redshift survey.

6. Summary

The search pipeline of the SDSS-II SN Survey has enabled efficient discoveries of variable and transient astronomical sources, filtering over 375,000 objects detected each season into several thousands of SN candidates. A reliable photometric SN typing system and spectroscopic follow-up algorithm have allowed spectroscopic observations of ~ 150 SNe Ia per season with 90% targeting efficiency. After two seasons, the search and spectroscopic follow-up algorithms have reached a relatively mature stage, and it is unlikely that major changes will be made for the third and final season of 2007. If the observing conditions resemble those of the previous two years, we expect to increase our sample of spectroscopically confirmed SN Ia by an additional $\sim 150 - 200$ events, reaching a sample of ~ 500 confirmed SNe Ia for the completed survey. A majority of the low-redshift sources will have well-sampled multi-band light curves that can serve as templates for future studies.

Spectroscopic target selection by a human is appropriate (and preferred) for a relatively small survey like the SDSS-II SN survey, but this is unlikely to be feasible for future large-scale surveys that will discover thousands or tens of thousands of SNe over the period of a few years. Based on our experience, however, we believe that much of the candidate identification process can be automated, and with just 2 – 4 epochs of multi-band imaging, SN candidates can be assigned probabilities that are reliable enough for performing follow-up spectroscopy. More quantitative studies of SN identification using photometric data alone will be presented in a future article.

Funding for the SDSS and SDSS-II has been provided by the Alfred P. Sloan Foundation, the Participating Institutions, the National Science Foundation, the U.S. Department of Energy, the National Aeronautics and Space Administration, the Japanese Monbukagakusho, the Max Planck Society, and the Higher Education Funding Council for England. The SDSS Web Site is `http://www.sdss.org/`.

The SDSS is managed by the Astrophysical Research Consortium for the Participating Institutions. The Participating Institutions are the American Museum of Natural History, Astrophysical Institute Potsdam, University of Basel, Cambridge University, Case Western Reserve University, University of Chicago, Drexel University, Fermilab, the Institute for Advanced Study, the Japan Participation Group, Johns Hopkins University, the Joint Institute for Nuclear Astrophysics, the Kavli Institute for Particle Astrophysics and Cosmology, the Korean Scientist Group, the Chinese Academy of Sciences (LAMOST), Los Alamos National Laboratory, the Max-Planck-Institute for Astronomy (MPIA), the Max-Planck-Institute for Astrophysics (MPA), New Mexico State University, Ohio State University, University of Pittsburgh, University of Portsmouth, Princeton University, the United States Naval Observatory, and the University of Washington.

The Hobby-Eberly Telescope (HET) is a joint project of the University of Texas at Austin, the Pennsylvania State University, Stanford University, Ludwig-Maximillians-Universität München, and Georg-August-Universität Göttingen. The HET is named in honor of its principal benefactors, William P. Hobby and Robert E. Eberly. The Marcario Low-Resolution Spectrograph is named for Mike Marcario of High Lonesome Optics, who fabricated several optics for the instrument but died before its completion; it is a joint project of the Hobby-Eberly Telescope partnership and the Instituto de Astronomía de la Universidad Nacional Autónoma de México. The Apache Point Observatory 3.5-meter telescope is owned and operated by the Astrophysical Research Consortium. We thank the observatory director, Suzanne Hawley, and site manager, Bruce Gillespie, for their support of this project. The Subaru Telescope is operated by the National Astronomical Observatory of Japan. The William Herschel Telescope is operated by the Isaac Newton Group, and the Nordic Optical Telescope is operated jointly by Denmark, Finland, Iceland, Norway, and Sweden, both on the island of La Palma in the Spanish Observatorio del Roque de los Muchachos of the Instituto de Astrofisica de Canarias. Observations at the ESO New Technology Telescope at La Silla Observatory were made under programme IDs 77.A-0437, 78.A-0325, and 79.A-0715. Kitt Peak National Observatory, National Optical Astronomy Observatory, is operated by the Association of Universities for Research in Astronomy, Inc. (AURA) under cooperative agreement with the National Science Foundation. The WIYN Observatory is a joint facility of the University of Wisconsin-Madison, Indiana University, Yale University, and the National Optical Astronomy Observatories. The W.M. Keck Observatory is operated

as a scientific partnership among the California Institute of Technology, the University of California, and the National Aeronautics and Space Administration. The Observatory was made possible by the generous financial support of the W.M. Keck Foundation. The South African Large Telescope of the South African Astronomical Observatory is operated by a partnership between the National Research Foundation of South Africa, Nicolaus Copernicus Astronomical Center of the Polish Academy of Sciences, the Hobby-Eberly Telescope Board, Rutgers University, Georg-August-Universität Göttingen, University of Wisconsin-Madison, University of Canterbury, University of North Carolina-Chapel Hill, Dartmough College, Carnegie Mellon University, and the United Kingdom SALT consortium.

A. Supernova Software

This appendix describes the details of the supernova software that runs on the computer cluster at APO.

The majority of `Framesub` is written in the `Perl` language. This provides the internal glue that strings together the various processing steps. In general, the image-level computations are written in the `C` language. These applications are called by the `Perl` scripts. The implementation of `Framesub` on the computing cluster is controlled by shell scripts.

As a programmatic summary, the `Framesub` pipeline consists of a series of *stages*, each of which has *actions* which it undertakes, as well as *dependencies* on the successful completion of previous stages. By default, an ensemble of images is passed from stage to stage using input and output lists. If an image fails the assigned actions in a particular stage, the frame is *not* passed into the input list for the subsequent stages of processing. A record is kept of the fact that it failed, and all such failures must be addressed individually. Below we describe the three modes in which the pipeline is run.

A.1. `sdssred`

This mode performs the basic reduction and preparation of the data for image subtraction.

- `FINDNEWIM`: After processing by `Photo`, `Framesub` must initialize its input list of images. This stage searches for the correct data products[16] for the camera column–filter combination assigned to it. This includes the `fpC` science image, a `fpM` mask image, an `asTrans` file providing the astrometry, and a `psField` file that contains `Photo`'s model of the PSF (Stoughton et al. 2002).

- `MKSATMASK`: The `fpM` file contains a pixel–by–pixel mask corresponding to any operations that have happened on the science image. This includes interpolation over CCD defects and cosmic rays, the masking of saturated pixels, and interpolation over bleed trails from the saturated stars. This stage translates the SDSS–format mask file into a mask image understood by `Framesub`. In practice, this is merely a reassignment to the numerical values of the mask bits.

[16] http://www.sdss.org/dr6/dm/flatFiles/FILES.html

We provide an additional level of editing in these images by masking halos around clusters of saturated pixels, as well as extending diffraction spike masks at the orientation correct for the camera rotation. These additional masks are only added for clusters of more than 20 saturated pixels. An operational scale length r for the halo and diffraction masking is determined by using the number of saturated pixels $N_{\rm sat}$ and solving for r through $N_{\rm sat} = \pi r^2$.

- `SDSSPSF`: This stage converts the solution for the PSF obtained by `Photo` contained in the `psField` files, into a format readable by `Dophot` (Schechter et al. 1993). The `Photo` PSF solution is later used to make an aperture correction to the difference image photometric measurements (see section A.3).

- `SDSSSTARS`: This stage obtains a list of the positions, magnitudes, and magnitude errors for the calibration stars contained within the frame and stores them in a text file suitable as input to `SDSSZERO`, which computes the zeropoints of each of the frames (see below). The list of calibration stars is also an optional input to `DIFFIM`, providing a list of preferred sources to be used in deriving the optimal convolution kernel (see section A.3). The magnitudes and magnitude errors were initially based on the DR4 database (Adelman-McCarthy et al. 2006), but were later updated based on the catalog provided by Ivezić et al. (2007).

  The difference images obtained by the SN Survey are always photometrically scaled to the template image; the following two stages are included when running `sdssred` on the template images.

- `STARDOPHOT`: This stage performs doPhot photometry on a list of calibration stars provided by `SDSSSTARS`, using the modified version of the `Dophot` software package.

- `SDSSZERO`: This stage performs zeropointing of the frame. The magnitudes and magnitude errors of the calibration stars are first converted to flux units via $10^{-0.4m}$, and then the model, ADU counts = A*flux, is solved for A using the weighted least-squares procedure. The zeropointing algorithm does iterative sigma clipping at $\{24.0, 12.0, 6.0, 6.0, 6.0\}$ standard deviations from the best fit zeropoint model. The final zeropoint, the statistical error on the zeropoint, and the RMS of the zeropoint are then converted into magnitudes and stored for use during the SN search.

A.2. `sdssred` With Fakes

To monitor the software and human search efficiencies, we insert artificial SNe (fakes) into the data stream in real-time. Prior to the beginning of the survey, a library of fakes

was generated (1000 fakes in 2005). Each fake is assigned a redshift, celestial position (α, δ), date of peak-magnitude in V band, and an intrinsic luminosity. The redshift distribution was generated according to $dN/dz \propto z^2$ and the celestial positions are then chosen to be near to a galaxy with the same redshift, based on a catalog of photometric redshifts (Oyaizu et al. 2007).

The fakes generated during the 2005 observing campaign did not include extinction and reddening; however the set of fakes generated during the 2006 campaign included extinction, with A_V chosen from an exponential distribution, $P(A_V) \propto e^{-A_V/0.4}$.

The following stages are used to generate realistic Type Ia SN light curves for the fakes in real time.

- `SDSSFAKESELECT`: To minimize computation time for inserting fakes into the data stream and still retain the ability to simulate the magnitude at an arbitrary light-curve epoch, a range of dates for which the fake magnitude is within the expected limit of the SDSS telescope was computed. This stage checks the library of fakes to see whether any fake has a position within the limits of the field and that the present MJD falls within the expected range of observability.

- `STARDOPHOT_FAKE`: This stage performs `Dophot` photometry on calibration stars within the frame. This is necessary to dynamically derive the magnitude to ADU conversion for the fakes.

- `SDSSZERO_FAKE`: This stage computes a zeropoint for the frame, based on the dophot photometry from the previous stage. It is identical to the `SDSSZERO` stage described in section A.1.

- `SDSSFAKEINSERT`: This stage inserts the fake SNe into the search image. Given the current MJD and the fake light-curve parameters described above, the theoretical magnitude is computed in real-time. The light-curve model is identical to the stretch model used for online photometric typing, as described in § 3.1. Given the magnitude and the zeropoint computed above, an integrated flux value is computed. The PSF model for the fake comes from the `Photo` derived PSF; this is remapped to the astrometric grid of the search image and photometrically scaled. Poisson noise is added to each pixel. Finally, the unperturbed search image is copied and the ADU values for each pixel are overlaid on the search image, which is passed to the subsequent processing stages. A record of changes to the image is written to the `fpC` file header, and the magnitudes and corresponding MJD are written to a `MySQL` database.

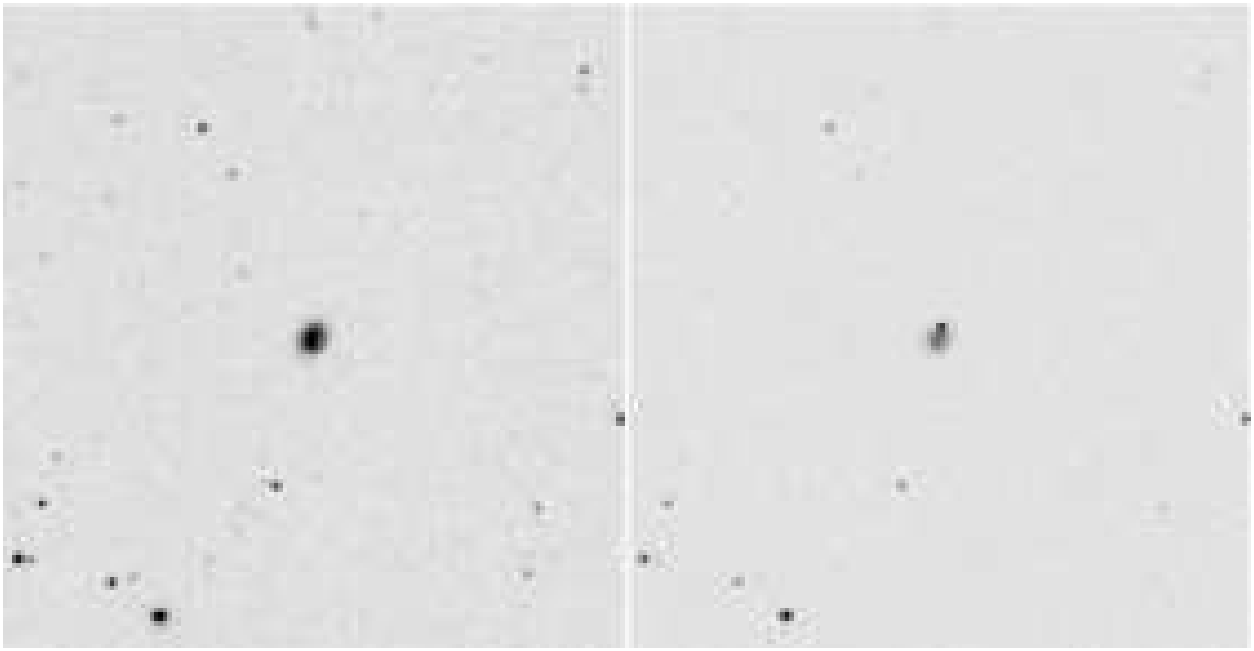

Fig. 9.— Template (left) and search (right) r-band images centered on the host galaxy of SN2005ir, a Type Ia SN at $z = 0.076$. The SN is visible above and slightly to the right of the of the host galaxy in the right-hand image. The search image was part of run 5823, and was taken under photometric conditions with $\sim 1.1''$ seeing. Images are $3.3'$ on the side. Note the enhanced density of faint sources ($r \gtrsim 23$ mag) visible in the template image that are not detected in the search image.

A.3. `sdssdiff`

This operational mode works with two sets of images that have been successfully run through the `sdssred` stages. One set of data is considered the "template" for difference imaging, and they are subtracted from the science images to yield only those objects that have varied in position or brightness.

In practice, most of our template images consist of the PSF–optimized coadds of SDSS Stripe 82 (Annis et al. 2006). The images consist of 5 – 10 coadded exposures, depending on the position in the stripe, from runs prior to the 2005 SN search season. Only images with seeing $\lesssim 1.1''$ are used. Figure 9 shows an r-band coadd image of the field around SN2005ir in comparison with a single-exposure search image. Some of our fields near the edge of the stripe fall outside of the coadd, and for these we use single–epoch templates from a night with good seeing.

- `MATCHTEMPL`: Since the SDSS camera is used in drift-scan mode, the data from a given run comprises a long swath of the sky. This tapestry is split by `Photo` into individual fields of 2048×1489 pixels, with 128 pixels of overlap between neighboring fields. Because Stripe 82 is an equatorial field, this corresponds to a slice in α. It is not guaranteed that the α boundaries of the science image agree exactly with those of the template, meaning in general we will need to identify and combine the two template images that overlap the science image. However, the pointing model of the telescope is sufficiently accurate that the overlap in δ is nearly complete.

- `GLUETEMPL`: This stage implements the pixel–level coaddition of the overlapping template images into a single template image whose RA coverage is similar to the input science image.

- `REMAP`: Because the images may still be misaligned in RA by a fractional pixel offset, and in declination by multiple pixels, we apply a remapping kernel that *exactly* aligns the glued template image with the science image. For this operation, we use the astrometry included in the `asTrans` files to determine, for each pixel in the science image, what position in the template image needs to be resampled. We apply a windowed–sinc resampling of the template image with a 9×9-pixel footprint (i.e., a Lanczos 4 kernel) to yield a final remapped glued template image. The template is always remapped to the reference frame of the science image, to avoid convolving the science data. Because the template image generally has much higher signal–to–noise (except possibly near the beginning of the stripe where only single-exposure templates are available), the "smoothing" effects due to convolution are not a serious issue. We propagate the pixel noise and pixel masks through this convolution process.

- `DIFFIM`: After the *astrometric* registration described above, we implement a *photometric* registration that matches the PSF of the two images, so that they may be subtracted on a pixel–by–pixel basis. This uses a modified version of the Alard (2000) algorithm as described in Becker et al. (2004).

  In this procedure, known objects (stars or galaxies) are used to determine a set of convolution kernels that minimize the difference between each convolved template object and the respective science object. Objects that include masked pixels are rejected, as are variable objects. The ensemble of kernels is then used to construct a single kernel function that varies spatially with position on the image, to account for differences in the PSF across the frames. This function is allowed to vary quadratically across the image. We then apply this kernel to each pixel in the image and subtract the convolved template from the science image, yielding a difference image in which the static signal has been subtracted, and only objects that have varied in position or brightness

remain. We choose to always apply this kernel to the template image, even though in good seeing conditions this requires us to actually *de*convolve the template data. We propagate the image noise and mask similar to the `REMAP` process.

- `DIFFDOPHOT`: We next perform object detection on the difference image, again using the modified `Dophot` package. The software is able to read the propagated noise and mask images to assist in the object detection and measurement. The background is explicitly set to zero, assuming that the difference imaging has produced a background–subtracted image. The `Photo` PSF model and aperture corrections are used to perform the photometry. We only perform photometry on positive–going excursions, thus objects that fade in brightness are not measured.

- `PIXCHK`: We next read in the difference, noise, and mask images surrounding each detected object and examine the neighboring pixels. The total *number* of positive–valued pixels, negative–valued pixels, and masked pixels are calculated in an aperture, as well as the total *amount* of flux in positive–valued and negative–valued pixels. These will be used to reject dipoles due to image misalignment or general failures in the difference imaging.

- `DIFFCUT`: This stage rejects candidates from the photometry list based upon photometry flags and `PIXCHK` values. In particular, objects for which `Dophot` is unable to perform a 4–parameter fit using the mean PSF parameters are rejected (`Dophot` types 4 or 6). Objects with S/N smaller than 3.0 are also rejected, as well as objects with excessive fractions of masked pixels (0.6) or fractions of flux in negative pixels (0.65), amongst other tests. These cuts yield the set of objects ingested into the database by `DoObjects`.

A.4. `sdssforce`

This mode is used to perform forced–positional PSF photometry. The coordinates of the candidate are determined from a S/N–weighted average of all objects associated with the SN. The PSF model is adopted from output of `Photo`. In practice, this mode is used to measure magnitudes in the u and z bands, which are not automatically processed by `sdssdiff`, as well as $ugriz$ magnitudes in images obtained before the SN discovery to obtain measurements of low-S/N detections and upper limits. This mode yields more accurate measurements of the fluxes than those produced by `sdssdiff`, and they generally agree with the final photometry to within ~ 0.05 mag in all filters (Holtzman et al. 2007).

B. Autoscanner

As a further illustration of the histogram method of PDF estimation, we note that Bayes' theorem, applied to classification, says that,

$$\frac{P(c_i|\theta)}{P(c_j|\theta)} = \frac{P(\theta|c_i)P(c_i)}{P(\theta|c_j)P(c_j)} \tag{B1}$$

where $P(a|b)$ is the conditional probability for a given b, c_i represents object class i, and θ denote particular values for the set of observables of an object. If this ratio is larger than one, then the object is more likely to belong to class i than to class j.

Applied to the problem at hand, this can be written as,

$$\frac{P(c_i|\theta)}{P(c_j|\theta)} = \frac{(N_i'/N_i)(N_i/N)}{(N_j'/N_j)(N_j/N)} = \frac{N_i'}{N_j'} \tag{B2}$$

where N_i is the total number of objects in the training set belonging to class i, N is the number of total objects in the training set, and a $'$ denotes objects possessing observables θ. The θ represents a subset of all possible observables, which is equivalent to marginalizing over all other observables, and the set used differs according to which class of background is being tested.

The criterion used by the autoscanner to identify objects of class i is,

$$\frac{N_i'}{N_j'} > \frac{N_i}{N_j} \tag{B3}$$

where i represents the classes of background (artifact, mover, dipole), and class j is always taken as SN. The motivation for this criterion is that we are searching for an *overdensity* of objects of class i in the region of observable space in question. In practice the threshold is a free parameter that can be adjusted to control the relative level of accepted signal to background events.

In this experiment, background events dominate over SNe epochs by a large factor, and a Bayesian classifier would reject SN epochs that lie in a reasonable region of the observable space if the region overlaps with background events, even far away from the peak of the background distribution. A cartoon of the situation is shown in Figure 10. Thus, the autoscanner can also be regarded as a Bayesian classifier where the thresholds are adjusted *a priori* to mitigate false negatives, at the cost of more background in the scanning.

The training set for the autoscanner consists of all objects from the 2005 observing season that were ranked by a human as an artifact, a dipole, a moving object, or a SN. This

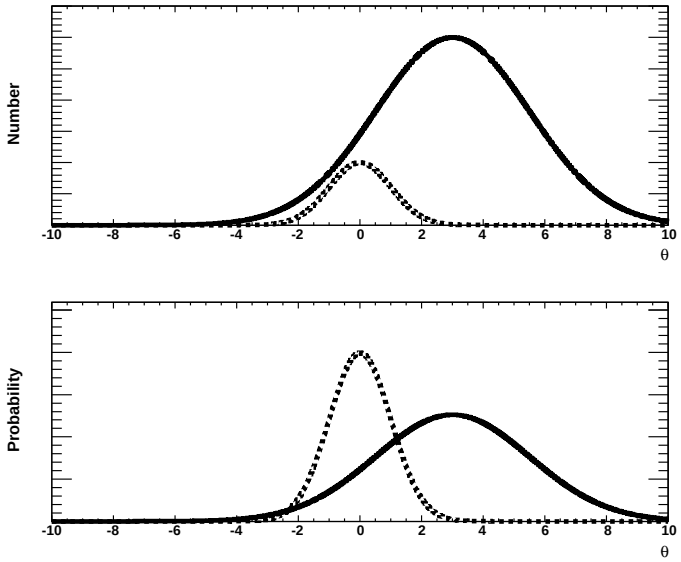

Fig. 10.— Hypothetical distributions of an observable for signal (dashed) and background (solid). The peak of the signal occurs at 0; however, the vastly greater number of background events swamps the signal. While it is true that an object with a value of this observable of 0 is more likely to be a background event, this is clearly not the behavior we want from our classifier, as we are trying to isolate the relatively rare signal events (i.e. SN epochs). The effect of recasting the problem from one of relative probabilities to one of overdensities. The peak of the signal (dashed) is now strongly inconsistent with background.

set is comprised of 91220 total objects, of which 65576 are a sub-class of background, and 25644 are objects ranked as a SN. The quantities used for classification of artifacts are, a measure of the objects ellipticity, the signal-to-noise ratio and the value of the reduced χ^2 when fitting the object to a model of the PSF. In computing the χ^2, we do not account for possible error in the PSF model and so objects with large signal-to-noise values also have large chi^2 values. Therefore, in classifying artifacts it is important to retain the correlation between chi^2 and signal-to-noise ratio. The quantities used for classifying dipoles are the measured flux in negative valued pixels, and the ratio of measured flux in negative valued pixels to the flux in positive valued pixels. The quantities used for classifying moving objects are the measured magnitudes, the magnitude of the apparent motion between different filters, and an angle describing the apparent motion between filters. If the object has a detection in the 3 filter-bands gri, then the angle is the angle between the "vector" that describes the apparent motion between the r and i filters, and the "vector" that describes the apparent motion between the i and g filters. If the object is truly moving then these apparent motions

should be nearly co-linear. If the object is only detected in 2 of the *gri* filters then the angle is the angle between the apparent motion between the 2 filters and the "unit vector" aligned in the direction of increasing right-ascension. Main-belt asteroids typically have an apparent motion in a fixed direction, and using this angle in the classification is a way to encode that information.

C. SN Ia Light Curve Models

This appendix describes the SN Ia light curve models used for photometric typing, redshift estimate, and selection of targets for spectroscopic observations. To calculate synthetic light curves of Branch-normal SNe Ia at various values of $\Delta m_{15}(B)$, the B-band magnitude change in 15 days from B-band maximum (Phillips 1993), we adopt the results of Phillips et al. (1999), who found relationships between the peak absolute BVI magnitudes of nearby SNe Ia as a function of $\Delta m_{15}(B)$. These authors parameterize the peak magnitude relative to that of a reference SN Ia with $\Delta m(B) = 1.1$ using a quadratic function of the form,

$$\Delta M_{\rm max} = a \times [\Delta m_{15}(B) - 1.1] + b \times [\Delta m_{15}(B) - 1.1]^2. \quad \text{(C1)}$$

There are a and b coefficients for each of the BVI filters, as listed in Table 3 of Phillips et al. (1999). The a coefficients ($a_B = 0.79$, $a_V = 0.67$, and $a_I = 0.42$) decrease as a function of the filter effective wavelength. This shows that SNe Ia with larger $\Delta m_{15}(B)$ are dimmer and redder; those with smaller $\Delta m_{15}(B)$ are intrinsically more luminous and bluer. We find that the a coefficient as a function of wavelength can be well-represented by the following linear relation,

$$a(\lambda) = 1.248 - 1.045 \times 10^{-4}\ \lambda(\text{Å}). \quad \text{(C2)}$$

We use this relation to perform color corrections directly onto the template spectra. Operationally, defining $F_\nu(\lambda, x = 0)$ to be the monochromatic flux (erg cm^{-2} s^{-1} Hz^{-1}) of the standard template spectrum at rest-frame wavelength λ, then the luminosity-corrected value is given by,

$$F_\nu(\lambda, x) \longrightarrow F_\nu(\lambda, x = 0) \times 10^{-0.4\ (ax + bx^2)}, \quad \text{(C3)}$$

where $x \equiv \Delta m_{15}(B)\ -1.1$, $b = 0.633$ (Phillips et al. 1999), and a is given in Equation C2. Although this color correction is valid at B-band maximum, we assume that it is valid at all epochs. This provides a way to compute synthetic light curves in the *ugriz* system (or any other filter set) for a SN Ia with a given $\Delta m_{15}(B)$ at arbitrary redshifts.

Finally, we stretch the light curves according to the method described in Perlmutter et al. (1997). The Nugent templates folded through the B-band filter transmission curve yield

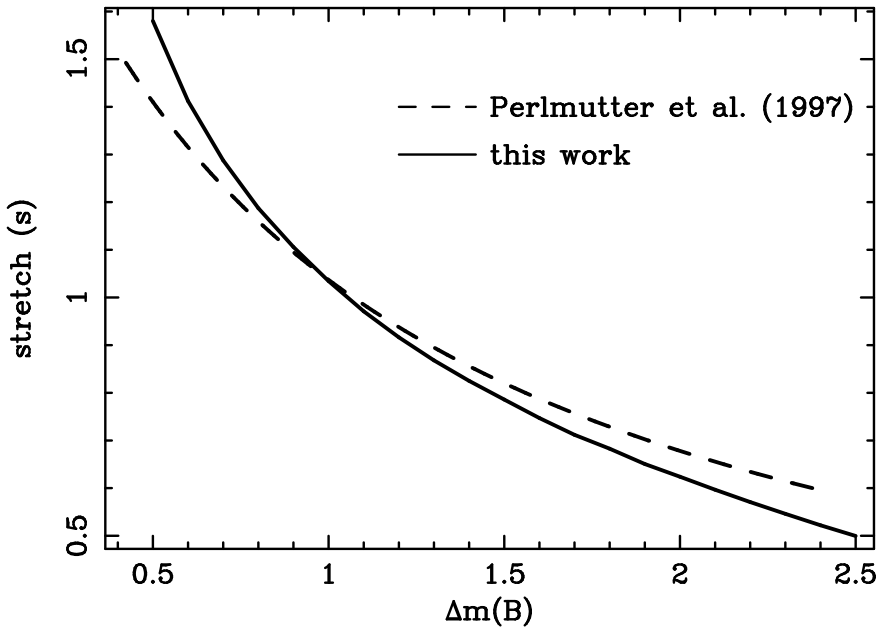

Fig. 11.— The stretch factor s at $z = 0$ as a function of $\Delta m_{15}(B)$ adopted in this work (black) in comparison to that of Perlmutter et al. (1997) represented by a dashed line.

$\Delta m_{15}(B) = 1.05$, so we define s to be unity when $\Delta m_{15}(B) = 1.05$. For other values of $\Delta m_{15}(B)$, we express the stretch factor as $s = (1 + z)\ (15/\tau)$, where we have factored out the cosmological time delay factor, and τ is represented by the following 3rd-order polynomial,

$$\tau[\Delta m(B)] = c_0 + c_1\ \Delta m_{15}(B) + c_2\ [\Delta m_{15}(B)]^2 + c_3\ [\Delta m_{15}(B)]^3, \qquad \text{(C4)}$$

where $c_0 = 3.455$, $c_1 = 13.719$, $c_2 = -3.601$, and $c_3 = 0.946$. This gives an adequate representation of the B-band light curve for $\Delta m_{15}(B)$ between 0.5 and 2.5. This function $s[\Delta m_{15}(B)]$ at zero redshift is plotted in Figure 11. The same relation derived by Perlmutter et al. (1997) is also shown for comparison. Figure 12 shows rest-frame g-band light curves for different values of $\Delta m_{15}(B)$. Peak absolute magnitudes in *ugriz* as function of $\Delta m_{15}(B)$ are shown in Figure 13.

Although this procedure does not always accurately reproduce the multi-band light curves, most notably the variation of the secondary peak in the red with $\Delta m_{15}(B)$ (Riess et al. 1996), they appear to be of sufficient quality for the purposes of photometric typing.

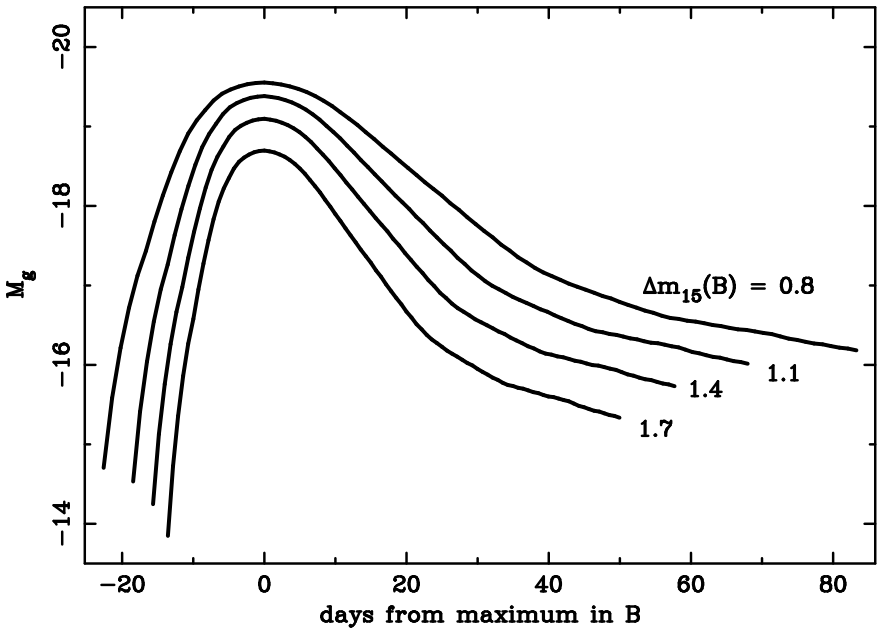

Fig. 12.— Sample SN Ia rest-frame g-band light curves for four values of $\Delta m_{15}(B) = 0.8, 1.1, 1.4$, and 1.7.

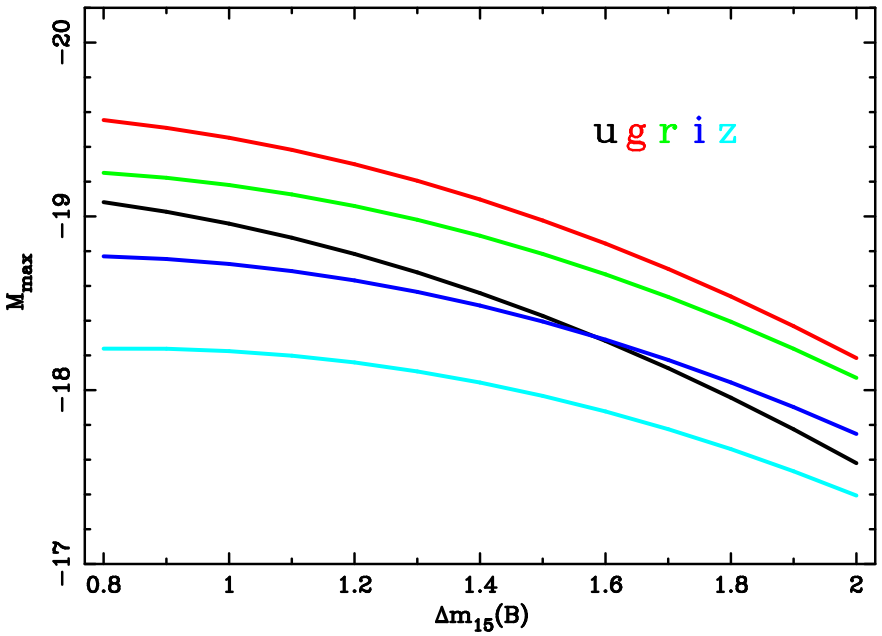

Fig. 13.— Resulting peak absolute magnitudes for a SN Ia at zero redshift in the SDSS *ugriz* system as functions of $\Delta m_{15}(B)$. The curves are analogous to those shown in Figure 8 of Phillips et al. (1999).

REFERENCES

Adelman-McCarthy, J. K., et al. 2006, ApJS, 162, 38

Adelman-McCarthy, J., et al. 2007, ApJS, in press

Adelman-McCarthy, J., et al. 2007, ApJS, submitted

Alard, C. 2000, A&AS, 144, 363

Aldering, G., et al. 2002, Proc. SPIE, 4836, 61

Annis, J. T., et al. 2006, American Astronomical Society Meeting Abstracts, 209, #215.09

Astier, P., et al. 2006, A&A, 447, 31

Barbary, K., et al. 2006, Bulletin of the American Astronomical Society, 38, 1025

Becker, A. C., et al. 2004, ApJ, 611, 418

Dilday, B., et al. 2007, in preparation

Filippenko, A. V. 1997, ARA&A, 35, 309

Filippenko, A. V., Li, W. D., Treffers, R. R., & Modjaz, M. 2001, IAU Colloq. 183: Small Telescope Astronomy on Global Scales, 246, 121

Frieman, J. et al. 2007, AJ, submitted

Fukugita, M., Ichikawa, T., Gunn, J. E., Doi, M., Shimasaku, K., & Schneider, D. P. 1996, AJ, 111, 1748

Gunn, J. E., et al. 1998, AJ, 116, 3040

Gunn, J. E., et al. 2006, AJ, 131, 2332

Hamuy, M., et al. 1993, AJ, 106, 2392

Hamuy, M., Phillips, M. M., Suntzeff, N. B., Schommer, R. A., Maza, J., & Aviles, R. 1996, AJ, 112, 2391

Hamuy, M., Phillips, M. M., Suntzeff, N. B., Schommer, R. A., Maza, J., & Aviles, R. 1996, AJ, 112, 2398

Hamuy, M., et al. 1996, AJ, 112, 2408

Hamuy, M., Phillips, M. M., Suntzeff, N. B., Schommer, R. A., Maza, J., Smith, R. C., Lira, P., & Aviles, R. 1996, AJ, 112, 2438

Hamuy, M., et al. 2006, PASP, 118, 2

Hogg, D. W., Finkbeiner, D. P., Schlegel, D. J., & Gunn, J. E. 2001, AJ, 122, 2129

Holtzman, J. et al., 2007, in preparation

Hsiao, E. Y., Conley, A., Howell, D. A., Sullivan, M., Pritchet, C. J., Carlberg, R. G., Nugent, P. E., & Phillips, M. M. 2007, ApJ, 663, 1187

Ivezić, Ž., et al. 2004, Astronomische Nachrichten, 325, 583

Ivezić, Ž., Allyn Smith, J., Miknaitis, G., Lin, H., & Tucker, D. 2007, ArXiv Astrophysics e-prints, arXiv:astro-ph/0703157

Jha, S., et al. 2006, AJ, 131, 527

Jha, S., Riess, A. G., & Kirshner, R. P. 2007, ApJ, 659, 122

Johnson, B. D., & Crotts, A. P. S. 2006, AJ, 132, 756

Kasen, D., & Woosley, S. E. 2007, ApJ, 656, 661

Kessler, R., et al. 2007, in preparation

Kim, A., Goobar, A., & Perlmutter, S. 1996, PASP, 108, 190

Kunz, M., Bassett, B. A., & Hlozek, R. A. 2007, Phys. Rev. D, 75, 103508

Kuznetsova, N. V., & Connolly, B. M. 2007, ApJ, 659, 530

Lupton, R., Gunn, J. E., Ivezić, Z., Knapp, G. R., & Kent, S. 2001, Astronomical Data Analysis Software and Systems X, 238, 269

Lupton, R. H., Ivezic, Z., Gunn, J. E., Knapp, G., Strauss, M. A., & Yasuda, N. 2002, Proc. SPIE, 4836, 350

Miknaitis, G., et al. 2007, ArXiv Astrophysics e-prints, arXiv:astro-ph/0701043

Nugent, P., Kim, A., & Perlmutter, S. 2002, PASP, 114, 803

Oyaizu, H., et al. 2007, in preparation

Perlmutter, S., et al. 1997, ApJ, 483, 565

Perlmutter, S., et al. 1999, ApJ, 517, 565

Pier, J. R., Munn, J. A., Hindsley, R. B., Hennessy, G. S., Kent, S. M., Lupton, R. H., & Ivezić, Ž. 2003, AJ, 125, 1559

Phillips, M. M. 1993, ApJ, 413, L105

Phillips, M. M., Lira, P., Suntzeff, N. B., Schommer, R. A., Hamuy, M., & Maza, J. 1999, AJ, 118, 1766

Phillips, M. M., et al. 2007, PASP, 119, 360

Poznanski, D., Gal-Yam, A., Maoz, D., Filippenko, A. V., Leonard, D. C., & Matheson, T. 2002, PASP, 114, 833

Poznanski, D., Maoz, D., & Gal-Yam, A. 2006, ArXiv Astrophysics e-prints, arXiv:astro-ph/0610129

Prieto, J., Anderson, S., Becker, A., Marriner, J., Sako, M., & Jha, S. 2006, Central Bureau Electronic Telegrams, 692, 1

Prieto, J. L., et al. 2007, in preparation

Pskovskii, I. P. 1977, Soviet Astronomy, 21, 675

Quimby, R., Höflich, P., & Wheeler, J. C. 2007, ArXiv e-prints, 705, arXiv:0705.4467

Riess, A. G., Press, W. H., & Kirshner, R. P. 1995, ApJ, 438, L17

Riess, A. G. 1996, Ph.D. Thesis

Riess, A. G., Press, W. H., & Kirshner, R. P. 1996, ApJ, 473, 88

Riess, A. G., et al. 1998, AJ, 116, 1009

Riess, A. G., et al. 1999, AJ, 117, 707

Riess, A. G., et al. 2004, ApJ, 607, 665

Riess, A. G., et al. 2004, ApJ, 600, L163

Riess, A. G., et al. 2007, ApJ, 659, 98

Sako, M., et al., in Proceedings of the 22nd Texas Symposium on Relativistic Astrophysics at Stanford, 2004, edited by P. Chen, E. Bloom, G. Madejski, and V. Petrosian, eConf C041213, 1424 (2005)

Schechter, P. L., Mateo, M., & Saha, A. 1993, PASP, 105, 1342

Shetrone, M., et al. 2007, PASP, 119, 556

Smith, C., Rest, A., Hiriart, R., Becker, A., Stubbs, C. W., Valdes, F. G., & Suntzeff, N. 2002, Proc. SPIE, 4836, 395

Smith, J. A., et al. 2002, AJ, 123, 2121

Stoughton, C., et al. 2002, AJ, 123, 485

Sullivan, M., et al. 2006, AJ, 131, 960

Tucker, D. L., et al. 2006, Astronomische Nachrichten, 327, 821

Wood-Vasey, W. M., et al. 2007, ArXiv Astrophysics e-prints, arXiv:astro-ph/0701041

York, D. G., et al. 2000, AJ, 120, 1579

Zheng, C. et al., 2007, in preparation

Table 1. Stripe 82 footprint

Strip	camcol	$\delta_{\rm min}$[a]	$\delta_{\rm max}$[a]
82N	1	$-1.058°$	$-0.833°$
···	2	$-0.638°$	$-0.413°$
···	3	$-0.219°$	$+0.007°$
···	4	$+0.201°$	$+0.426°$
···	5	$+0.621°$	$+0.846°$
···	6	$+1.041°$	$+1.266°$
82S	1	$-1.267°$	$-1.042°$
···	2	$-0.848°$	$-0.622°$
···	3	$-0.428°$	$-0.203°$
···	4	$-0.008°$	$+0.217°$
···	5	$+0.411°$	$+0.637°$
···	6	$+0.831°$	$+1.057°$

[a]These values correspond to the nominal δ values. The exact telescope pointing differs slightly from night to night resulting in a shift in δ by as much as $0.003°$ in either direction.

Table 2. 2005 SDSS Supernova Imaging Runs

Run	Strip	MJD_{start}	MJD_{end}	RA_{start}	RA_{end}
5566	N	53616.215	53616.469	−32.72	+58.91
5582	S	53622.207	53622.477	−40.36	+57.41
5590	N	53623.156	53623.324	−50.67	+9.96
5597	S	53625.176	53625.266	−50.62	−18.43
5603	N	53626.141	53626.449	−50.62	+60.17
5607	S	53627.137	53627.441	−50.59	+59.90
5610	N	53628.129	53628.434	−50.57	+60.21
5619	S	53634.129	53634.438	−50.68	+60.71
5622	N	53635.137	53635.445	−50.72	+60.66
5628	S	53636.133	53636.281	−50.70	+1.99
5633	N	53637.129	53637.371	−50.68	+36.45
5637	S	53638.254	53638.477	−20.72	+60.72
5642	N	53639.289	53639.484	−9.82	+60.69
5646	S	53640.234	53640.441	−13.85	+60.70
5654	N	53641.113	53641.121	−55.42	−53.02
5658	N	53641.359	53641.465	+16.08	+54.56
5666	S	53643.430	53643.484	+41.25	+60.71
5670	N	53644.109	53644.430	−55.53	+60.79
5675	S	53645.180	53645.219	−55.52	−41.75
5681	S	53646.418	53646.480	+29.97	+52.88
5698	S	53648.164	53648.289	−55.62	−9.81
5702	N	53649.102	53649.129	−55.55	−46.42
5709	N	53654.152	53654.359	−51.60	+23.25
5713	S	53655.094	53655.363	−55.54	+41.47
5719	N	53656.090	53656.246	−55.45	+1.14
5729	S	53657.203	53657.215	−46.95	−43.05
5730	S	53657.258	53657.324	+37.20	+60.71
5731	N	53657.332	53657.441	+21.17	+60.69
5732	S	53657.449	53657.488	+47.11	+60.73
5743	N	53663.086	53663.164	−55.42	−26.98
5744	N	53663.176	53663.418	−29.75	+57.83
5745	S	53663.430	53663.488	+33.09	+55.10
5754	S	53664.117	53664.367	−55.60	+34.37
5759	N	53665.082	53665.395	−55.52	+57.81
5760	S	53665.406	53665.492	+25.13	+55.68
5763	S	53666.082	53666.246	−55.49	+3.94
5765	N	53666.332	53666.480	+2.30	+54.86
5770	N	53668.094	53668.406	−55.54	+57.94
5771	S	53668.418	53668.492	+33.09	+60.79
5776	S	53669.078	53669.391	−55.50	+57.82
5777	N	53669.406	53669.496	+25.61	+57.96
5781	N	53670.098	53670.410	−55.31	+57.86
5782	S	53670.422	53670.500	+32.65	+60.66
5786	S	53671.273	53671.484	−14.82	+60.65
5792	N	53673.066	53673.379	−55.42	+57.91
5797	S	53674.062	53674.375	−55.57	+58.05

Table 2—Continued

Run	Strip	MJD_{start}	MJD_{end}	RA_{start}	RA_{end}
5800	N	53675.062	53675.371	−55.61	+56.07
5807	S	53676.172	53676.465	−47.67	+57.89
5808	N	53676.473	53676.496	+49.27	+57.96
5813	N	53677.082	53677.359	−55.56	+44.59
5820	S	53679.152	53679.441	−44.54	+59.96
5823	N	53680.070	53680.391	−55.46	+60.71
5836	S	53681.113	53681.438	−55.48	+60.70
5842	N	53683.129	53683.449	−55.43	+60.76
5847	S	53684.301	53684.398	+25.71	+60.74
5853	S	53685.062	53685.172	−58.95	−19.28
5864	N	53686.141	53686.152	−50.06	−45.42
5865	N	53686.172	53686.242	−42.96	−18.11
5866	N	53686.273	53686.391	+18.21	+60.73
5870	S	53687.109	53687.250	−55.57	−6.16
5871	S	53687.258	53687.340	+31.39	+60.74
5872	N	53687.352	53687.449	+25.14	+60.78
5878	N	53693.059	53693.395	−59.98	+60.68
5882	S	53694.074	53694.410	−60.11	+60.71
5889	S	53696.355	53696.402	+44.01	+60.78
5895	S	53697.059	53697.395	−60.11	+60.71
5898	N	53698.059	53698.129	−59.98	−33.63
5902	N	53699.082	53699.301	−60.13	+18.78
5905	S	53700.059	53700.391	−59.99	+60.69
5909	N	53702.059	53702.211	−59.35	−4.10
5915	N	53703.066	53703.156	−60.01	−27.07
5918	N	53704.059	53704.379	−54.46	+60.67
5924	S	53705.043	53705.379	−60.06	+60.76

Table 3. 2006 SDSS Supernova Imaging Runs

Run	Strip	MJD_{start}	MJD_{end}	RA_{start}	RA_{end}
6281	N	53974.141	53974.203	−56.82	−34.52
6283	N	53974.270	53974.336	−11.69	+12.42
6287	S	53975.133	53975.465	−58.78	+60.70
6293	N	53977.371	53977.387	+7.31	+13.45
6313	N	53989.121	53989.160	−60.05	−45.99
6314	N	53989.176	53989.473	−47.39	+60.70
6330	S	53990.312	53990.387	+1.17	+27.82
6348	S	53993.277	53993.371	−31.19	+2.94
6349	S	53993.379	53993.414	+26.11	+38.98
6353	S	53994.125	53994.156	−59.99	−48.77
6355	S	53994.301	53994.484	−5.78	+59.80
6360	N	53995.129	53995.254	−59.98	−14.92
6362	N	53995.344	53995.391	+9.13	+25.90
6363	N	53995.414	53995.453	+25.67	+40.04
6367	S	53996.168	53996.469	−47.82	+60.72
6370	N	53997.105	53997.199	−59.99	−26.15
6373	N	53997.352	53997.422	−17.22	+8.09
6374	N	53997.434	53997.469	+38.16	+50.88
6377	S	53998.105	53998.312	−60.00	+14.85
6383	N	54000.191	54000.430	−32.88	+53.50
6391	N	54003.145	54003.160	−60.06	−54.52
6400	N	54005.078	54005.160	−60.02	−30.98
6401	S	54005.168	54005.191	−50.90	−41.62
6402	S	54005.230	54005.332	−24.92	+11.76
6404	S	54005.383	54005.484	+24.97	+60.75
6408	S	54006.094	54006.125	−59.99	−48.77
6409	N	54006.137	54006.395	−32.79	+60.78
6412	N	54007.094	54007.191	−58.91	−24.18
6414	N	54007.258	54007.484	−25.93	+54.91
6417	S	54008.094	54008.430	−60.13	+60.68
6418	N	54008.438	54008.461	+53.21	+60.70
6421	N	54009.090	54009.422	−60.12	+60.69
6422	S	54009.434	54009.484	+37.09	+56.10
6425	S	54010.090	54010.426	−60.04	+60.77
6430	N	54011.152	54011.488	−60.10	+60.71
6433	S	54012.082	54012.418	−60.08	+60.73
6435	N	54012.434	54012.484	+36.09	+54.35
6441	N	54019.102	54019.289	−60.13	+6.64
6444	N	54019.371	54019.480	+21.13	+60.66
6447	S	54020.090	54020.367	−60.05	+40.10
6448	S	54020.395	54020.457	+39.08	+60.79
6450	N	54021.305	54021.492	−6.74	+60.79
6453	S	54022.137	54022.293	−60.01	−4.47
6458	S	54024.316	54024.492	−6.73	+55.85
6461	N	54025.152	54025.488	−60.11	+60.71
6464	S	54026.090	54026.133	−59.99	−45.02

Table 3—Continued

Run	Strip	MJD_{start}	MJD_{end}	RA_{start}	RA_{end}
6468	S	54028.078	54028.254	−60.06	+2.96
6471	S	54028.352	54028.492	+9.53	+60.74
6474	N	54029.082	54029.336	−60.05	+31.41
6476	N	54029.414	54029.496	+30.56	+60.66
6479	S	54030.082	54030.293	−60.09	+15.96
6480	S	54030.371	54030.445	+33.19	+59.24
6484	N	54031.070	54031.402	−60.01	+60.66
6488	S	54032.070	54032.164	−60.06	−26.83
6494	S	54034.137	54034.223	−61.51	−31.27
6501	S	54035.234	54035.492	−32.56	+60.72
6504	N	54036.074	54036.410	−60.00	+60.67
6508	S	54037.062	54037.398	−60.52	+60.59
6513	N	54039.070	54039.406	−60.08	+60.73
6518	S	54040.078	54040.414	−60.12	+60.69
6522	N	54041.074	54041.152	−60.00	−31.86
6524	N	54041.227	54041.379	+6.11	+60.75
6525	S	54041.387	54041.449	+39.12	+60.68
6528	S	54047.070	54047.164	−60.11	−25.23
6530	S	54047.254	54047.441	−7.98	+60.74
6533	N	54048.066	54048.344	−60.10	+39.61
6534	N	54048.367	54048.430	+38.70	+60.71
6537	S	54049.223	54049.438	−17.38	+60.78
6542	S	54050.062	54050.215	−59.99	−4.60
6545	S	54050.344	54050.398	+41.22	+60.68
6548	N	54051.059	54051.164	−60.03	−22.01
6552	N	54052.070	54052.406	−60.05	+60.77
6555	S	54053.070	54053.320	−60.02	+31.00
6556	S	54053.328	54053.418	+28.37	+60.71
6559	N	54054.090	54054.293	−60.06	+14.05
6564	N	54055.066	54055.316	−60.10	+30.18
6565	N	54055.328	54055.418	+28.17	+60.66
6568	S	54056.070	54056.406	−60.05	+60.77
6571	S	54057.055	54057.152	−53.76	−19.32
6577	N	54058.066	54058.398	−59.99	+60.68
6580	S	54059.066	54059.398	−60.06	+60.76
6584	N	54060.137	54060.422	−42.83	+60.78
6590	S	54061.074	54061.203	−60.09	−13.52
6592	S	54061.277	54061.410	+12.07	+60.73
6596	S	54062.070	54062.402	−60.07	+60.75
6600	N	54063.055	54063.320	−60.10	+34.82
6604	S	54064.309	54064.402	+27.24	+60.78
6609	N	54065.320	54065.398	+33.18	+60.73
6615	S	54068.059	54068.180	−60.05	−16.78
6618	S	54068.211	54068.387	−1.81	+60.77

Table 4. Reduction of 2006 Handscanning by Autoscanner

	number of objects
Total to be scanned[a]	145,428
1st epoch	118,584
Bright[b]	21,882
Scanned[c]	8,373
2nd epoch	26,844
Scanned	6,007
Total scanned[d]	14,430

[a]The number of objects that humans would have scanned in 2006 without the autoscanner.

[b]Objects that were detected for the first time and brighter than 21 mag in g or r.

[c]Actual number of "Bright", first-epoch objects that were scanned.

[d]Total number of objects scanned in 2006. This number differs slightly from the sum of the scanned first- and second-epoch objects because some scanners on a few occasions chose to scan first-epochs objects as faint as 21.5 mag in g or r.

Table 5. List of spectroscopically confirmed supernovae in 2005

Candidate ID[a]	IAU Name	z[b]	RA[c] (degrees in J2000)	Dec	Discovery Date	Type[d]	# of Spectra[e]
722	2005ed	0.0859	0.70569	+0.75127	2005-09-04	SN Ia	1
739	2005ef	0.1072	14.59529	+0.67906	2005-09-04	SN Ia	1
744	2005ei	0.1286	−30.80149	+0.31750	2005-09-04	SN Ia	1
762	2005eg	0.1912	15.53535	−0.87899	2005-09-04	SN Ia	1
774	2005ex	0.0936	25.46351	−0.87638	2005-09-04	SN Ia	2
1032	2005ez	0.1299	46.79571	+1.11953	2005-09-06	SN Ia	1
1112	2005fg	0.2585	−20.98238	−0.37519	2005-09-10	SN Ia	1
1114	2005lb	0.0257	−16.29145	−0.25250	2005-09-10	SN II	1
1119	2005fc	0.2982	−39.58644	+0.89466	2005-09-10	SN Ia	1
1166	···	0.3825	9.35564	+0.97328	2005-09-10	SN Ia	1
1241	2005ff	0.089	−22.32746	−0.77659	2005-09-10	SN Ia	2
1253	2005fd	0.2625	−36.20095	+0.16308	2005-09-10	SN Ia	2
1316	2005fe	0.2174	−25.13617	+0.49444	2005-09-10	SN Ia	1
1371	2005fh	0.1189	−10.62619	+0.42939	2005-09-10	SN Ia	1
1472	2005lc	0.0144	45.54660	−1.16651	2005-09-10	SN II	1
1580	2005fb	0.186	45.32310	−0.64409	2005-09-11	SN Ia	1
1686	···	0.1367	2.24835	−0.21039	2005-09-11	SN Ia?	1
1688	···	0.3591	−38.64223	+0.32454	2005-09-11	SN Ia	1
1794	2005fj	0.1426	−42.16314	−0.44537	2005-09-11	SN Ia	1
2000	2005hl	0.0243	−46.16752	+0.54298	2005-09-13	SN Ib	1
2017	2005fo	0.2629	−31.05666	+0.59352	2005-09-13	SN Ia	1
2030	2005fl	0.2343	−48.15841	−1.25328	2005-09-13	SN Ia	1
2031	2005fm	0.1530	−47.95680	−1.17143	2005-09-13	SN Ia	1
2053	2005fk	0.2651	−41.16734	−0.38295	2005-09-13	SN Ic	1
2102	2005fn	0.0958	−47.77902	+0.19114	2005-09-13	SN Ia	1
2165	2005fr	0.291	17.09174	−0.09627	2005-09-14	SN Ia	1
2246	2005fy	0.1952	50.09041	−0.88558	2005-09-14	SN Ia	4
2308	2005ey	0.149	34.27287	+0.28030	2005-09-14	SN Ia	3
2330	2005fp	0.2135	6.80711	+1.12060	2005-09-14	SN Ia	1
2366	2005fq	0.1462	13.43351	−0.56021	2005-09-15	SN II	1
2372	2005ft	0.1798	40.52072	−0.54085	2005-09-15	SN Ia	3
2422	2005fi	0.268	1.99454	+0.63820	2005-09-15	SN Ia	1
2440	2005fu	0.194	42.63370	+0.80780	2005-09-15	SN Ia	1
2533	2005fs	0.344	31.22069	−0.32647	2005-09-15	SN Ia	1
2561	2005fv	0.1170	46.34345	+0.85837	2005-09-15	SN Ia	4
2635	2005fw	0.1440	52.70433	−1.23808	2005-09-16	SN Ia	3
2661	···	0.1930	−6.79249	+0.09721	2005-09-16	SN II	1
2689	2005fa	0.166	24.90035	−0.75875	2005-09-16	SN Ia	1
2744	2005hm	0.0350	−35.24730	−1.02741	2005-09-16	SN Ib	1
2789	2005fx	0.2907	−15.79855	+0.40110	2005-09-17	SN Ia	1
2916	2005fz	0.121	−44.07830	+0.56956	2005-09-23	SN Ia	4
2943	2005go	0.2662	17.70495	+1.00792	2005-09-24	SN Ia	1
2992	2005gp	0.1266	55.49706	−0.78267	2005-09-24	SN Ia	2
3080	2005ga	0.1739	16.93234	−1.03950	2005-09-25	SN Ia	3
3087	2005gc	0.1654	20.40671	−0.97723	2005-09-25	SN Ia	2

Table 5—Continued

Candidate ID[a]	IAU Name	z[b]	RA[c] (degrees in J2000)	Dec	Discovery Date	Type[d]	# of Spectra[e]
3199	2005gs	0.2511	−26.70728	+1.05054	2005-09-25	SN Ia	1
3241	2005gh	0.387	−47.34854	−0.35409	2005-09-25	SN Ia?	1
3256	2005hn	0.1076	−30.73229	−0.22348	2005-09-25	SN Ia	1
3317	2005gd	0.1618	26.96261	+0.64061	2005-09-25	SN Ia	2
3331	2005ge	0.208	34.56138	+0.79656	2005-09-25	SN Ia?	2
3377	2005gr	0.2460	54.15620	+1.07917	2005-09-25	SN Ia	1
3451	2005gf	0.2498	−25.93073	+0.70815	2005-09-25	SN Ia	1
3452	2005gg	0.2313	−25.32850	+0.63919	2005-09-25	SN Ia	1
3592	2005gb	0.0870	19.05242	+0.79195	2005-09-26	SN Ia	3
3818	2005gi	0.0511	13.96950	+0.50494	2005-09-26	SN II	1
3901	2005ho	0.0638	14.85043	+0.00261	2005-09-26	SN Ia	2
4000	2005gt	0.2793	31.01601	−0.36583	2005-09-26	SN Ia	1
4012	···	0.0253	48.44893	−0.24360	2005-09-26	SN Ic	1
4046	2005gw	0.278	−5.50168	+0.64211	2005-09-26	SN Ia	1
4241	2005gu	0.3320	12.23769	−0.90573	2005-09-27	SN Ia	1
4524	2005gj	0.0618	45.29978	−0.55387	2005-09-28	SN Ia	19
4577	2005gv	0.365	38.47554	+0.28071	2005-09-28	SN Ia	1
4679	2005gy	0.3345	21.52834	+0.67686	2005-09-29	SN Ia	1
5103	2005gx	0.148	−0.11556	+0.73717	2005-10-02	SN Ia	2
5183	2005gq	0.3905	53.45402	+0.70935	2005-10-02	SN Ia	1
5350	2005hp	0.1764	−52.78083	−0.77924	2005-10-03	SN Ia	1
5391	2005hs	0.3009	52.34197	−1.09470	2005-10-03	SN Ia	1
5395	2005hr	0.1170	49.64095	+0.12335	2005-10-03	SN Ia	1
5533	2005hu	0.2206	−31.33006	+0.41343	2005-10-12	SN Ia	1
5549	2005hx	0.120	3.25054	+0.24823	2005-10-12	SN Ia	1
5550	2005hy	0.1562	3.59830	+0.33305	2005-10-12	SN Ia	3
5588	2005hw	0.4103	2.36862	+1.15492	2005-10-12	SN Ia	1
5635	2005hv	0.1795	−26.81724	−0.03492	2005-10-12	SN Ia	1
5717	2005ia	0.2545	17.89596	−0.00589	2005-10-12	SN Ia	1
5736	2005jz	0.2654	22.86274	−0.63162	2005-10-12	SN Ia	1
5737	2005ib	0.3937	22.85704	−0.60339	2005-10-12	SN Ia	1
5751	2005hz	0.1305	11.63416	+0.83823	2005-10-12	SN Ia	3
5821	2005hq	0.465	−47.41758	−0.82528	2005-10-13	SN Ia?	2
5844	2005ic	0.3118	−32.21379	−0.84294	2005-10-13	SN Ia	1
5916	2005is	0.1746	5.43739	−0.32503	2005-10-13	SN Ia?	3
5944	2005hc	0.0459	29.19980	−0.21372	2005-10-13	SN Ia	5
5957	2005ie	0.2803	34.76058	−0.27283	2005-10-13	SN Ia	2
5966	2005it	0.3090	16.19039	+0.51392	2005-10-13	SN Ia	1
5994	2005ht	0.189	−47.39745	−0.16789	2005-10-13	SN Ia	1
6057	2005if	0.0675	52.55362	−0.97458	2005-10-15	SN Ia	2
6100	2005ka	0.3186	−26.51685	+1.08649	2005-10-20	SN Ia	1
6108	2005ih	0.2603	1.80660	+0.34898	2005-10-21	SN Ia	1
6127	2005iw	0.2894	−22.67602	−0.09236	2005-10-21	SN Ia	1
6137	2005iv	0.3001	−52.06387	+0.24475	2005-10-21	SN Ia	1
6192	2005jy	0.2727	−11.53501	+1.25699	2005-10-21	SN Ia	1

Table 5—Continued

Candidate ID[a]	IAU Name	z[b]	RA[c] (degrees in J2000)	Dec	Discovery Date	Type[d]	# of Spectra[e]
6196	2005ig	0.2809	−22.36885	−0.50266	2005-10-21	SN Ia	1
6249	2005ii	0.2950	3.26555	−0.62012	2005-10-21	SN Ia	1
6295	2005js	0.0793	23.67298	−0.60537	2005-10-21	SN Ia	2
6304	2005jk	0.185	26.49762	+1.19596	2005-10-21	SN Ia	3
6315	2005ix	0.2557	−49.51717	+1.09200	2005-10-21	SN Ia	2
6406	2005ij	0.1240	46.08861	−1.06296	2005-10-22	SN Ia	2
6422	2005id	0.187	−10.86119	−0.66322	2005-10-22	SN Ia	1
6471	···	0.2018	−50.61388	+0.49495	2005-10-22	SN II	1
6558	2005hj[f]	0.0574	21.70167	−1.23812	2005-10-22	SN Ia	2
6649	2005jd	0.318	34.27586	+0.53484	2005-10-23	SN Ia	2
6696	···	0.2382	−20.92067	+0.47925	2005-10-23	SN Ia?	1
6699	2005ik	0.313	−37.18502	−1.05699	2005-10-23	SN Ia	2
6773	2005iu	0.0916	−54.93498	+0.21737	2005-10-24	SN Ia	1
6777	2005iy	0.4043	−38.78356	+0.38561	2005-10-24	SN Ia	2
6780	2005iz	0.206	−31.93139	+0.26708	2005-10-24	SN Ia	1
6852	2005jf	0.3007	53.41983	−0.11210	2005-10-24	SN Ia?	1
6924	2005ja	0.329	−1.03067	+0.87698	2005-10-24	SN Ia	1
6933	2005jc	0.214	11.35172	+1.07558	2005-10-24	SN Ia	2
6936	2005jl	0.1810	−36.76618	−0.69978	2005-10-24	SN Ia	1
6962	2005je	0.0930	38.86091	+1.07488	2005-10-24	SN Ia?	1
6968	···	0.0983	19.55569	−0.90655	2005-10-24	SN Ia?	3
7017	···	0.1430	31.36534	−0.49791	2005-10-24	SN Ia	3
7143	2005jg	0.306	−14.73764	−0.20737	2005-10-26	SN Ia	1
7147	2005jh	0.1099	−9.98155	−0.05548	2005-10-26	SN Ia	3
7243	2005jm	0.2045	−31.92092	+0.47193	2005-10-27	SN Ia	1
7335	2005kn	0.197	−41.11480	−0.35534	2005-10-27	SN Ia?	1
7426	2005jb	0.386	−20.98663	−0.36792	2005-10-27	SN Ia?	1
7460	2005jx	0.2133	−36.41594	−0.68170	2005-10-27	SN Ia?	1
7473	2005ji	0.220	4.32641	−0.25726	2005-10-27	SN Ia	2
7475	2005jn	0.3191	4.75348	−0.28149	2005-10-27	SN Ia	2
7512	2005jo	0.2354	52.09032	−0.32609	2005-10-27	SN Ia	1
7779	2005jw	0.376	−49.91979	−0.00717	2005-10-28	SN Ia	1
7847	2005jp	0.2126	32.45995	−0.06179	2005-10-28	SN Ia	1
7876	2005ir	0.0767	19.18251	+0.79463	2005-10-28	SN Ia	2
7947	2005jj	0.368	−45.81392	+0.40835	2005-10-28	SN Ia?	1
8030	2005jv	0.423	40.20883	+0.99314	2005-10-28	SN Ia	1
8046	2005ju	0.2591	39.11682	+0.51126	2005-10-29	SN Ia	1
8151	2005hk	0.0131	6.96200	−1.19815	2005-10-29	SN Ia	11
8213	2005ko	0.1855	−2.47907	−0.92139	2005-10-31	SN Ia	2
8495	2005mi	0.2151	−24.73898	−0.74816	2005-10-31	SN Ia	1
8598	2005jt	0.3613	42.66734	−0.06596	2005-11-01	SN Ia	1
8679	2005jr	0.2945	15.05152	+0.34081	2005-11-01	SN II	1
8707	2005mh	0.3951	41.23617	+0.20359	2005-11-01	SN Ia?	1
8719	2005kp	0.1174	7.72148	−0.71884	2005-11-01	SN Ia	2
8921	2005ld	0.1462	−34.99800	−0.00792	2005-11-02	SN Ia	2

Table 5—Continued

Candidate ID[a]	IAU Name	z[b]	RA[c] (degrees in J2000)	Dec	Discovery Date	Type[d]	# of Spectra[e]
9032	2005le	0.2549	−22.11544	−0.49357	2005-11-02	SN Ia	1
9045	2005kq	0.3903	−12.16286	−0.60863	2005-11-02	SN Ia	1
9118	2005kr	0.1344	47.12358	+0.88893	2005-11-03	SN Ic	1
9207	2005lg	0.3509	19.08363	−0.80780	2005-11-03	SN Ia	1
9273	2005ks	0.0992	−35.51432	−0.03245	2005-11-03	SN Ic	1
9457	2005li	0.2572	−24.18564	+0.25304	2005-11-04	SN Ia	1
9467	2005lh	0.2191	−31.04860	+1.18079	2005-11-04	SN Ia	2
10028	2005kt	0.0662	17.74185	+0.27615	2005-11-07	SN Ia	1
10096	2005lj	0.0789	29.42928	−0.17945	2005-11-07	SN Ia	1
10106	···	0.1479	47.69327	−0.20488	2005-11-07	SN Ia?	2
10297	2005mk	0.1486	−19.33066	+0.83301	2005-11-08	SN II	1
10367	2005kb	0.0155	12.71115	+0.85362	2005-11-08	SN II	2
10434	2005lk	0.1037	−30.04406	−1.19371	2005-11-08	SN Ia	1
10449	2005ll	0.246	−22.97138	−1.12817	2005-11-08	SN Ia	1
10550	2005lf	0.3008	−10.32462	−1.20487	2005-11-08	SN Ia	1
10805	2005ku	0.0456	−15.07246	−0.01371	2005-11-10	SN Ia	1
10907	2005lm	0.0853	3.77046	+0.35514	2005-11-12	SN II	1
11017	2005mj[g]	0.210	−37.04401	−1.06939	2005-11-13	SN II	1
11067	2005ml	0.119	33.51840	−0.23918	2005-11-14	SN Ia	1
11206	2005mm	0.3805	3.28979	+1.14552	2005-11-20	SN Ia	1
11300	2005ln	0.130	6.75050	−0.58662	2005-11-20	SN Ia	1
11320	2005mo	0.2743	57.55376	−0.24022	2005-11-22	SN Ia	1
11332	2005mn	0.0474	57.32682	−0.69207	2005-11-23	SN Ib	4
11452	2005lo	0.300	9.29943	−1.20342	2005-11-24	SN Ia	1
11557	2005lq	0.382	40.40017	+0.20502	2005-11-24	SN Ia	1
11650	2005mp	0.275	16.19032	+0.05563	2005-11-25	SN Ia	1
11864	2005lp	0.305	26.92832	+0.20722	2005-11-26	SN Ia	1
12136	2005mq	0.352	−9.90923	−0.34989	2005-11-27	SN Ia	1

[a]Internal SN candidate designation.

[b]Final spectroscopic redshifts. When narrow galaxy lines are detected in at least one of the spectra, the redshifts are given to four decimal places. The typical uncertainties are ~ 0.0005. When only the SN is detected, the redshifts are given to three decimal places and the uncertainties are ~ 0.005 (see Zheng et al. 2007).

[c]Right Ascension is provided in decimal degrees defined in the range [-180°,+180°].

[d]The final spectroscopic type of the SN candidate. Spectroscopically probable SNe Ia are designated "SN Ia?" (see Zheng et al. 2007).

[e]This includes all spectral observations performed including those of the SN candidate and possibly its host galaxy.

[f]Spectroscopically confirmed by Quimby et al. (2007).

[g]Spectroscopically confirmed by the ESSENCE Group.

Table 6. List of spectroscopically confirmed supernovae in 2006

Candidate ID[a]	IAU Name	z[b]	RA[c] (degrees in J2000)	Dec	Discovery Date	Type[d]	# of Spectra[e]
12778	2006fs	0.10	−42.50417	+0.40879	2006-08-27	SN Ia	1
12779	2006fd	0.08	−50.52813	+1.22112	2006-08-27	SN Ia	1
12780	2006eq[f]	0.05	−37.84531	+1.22811	2006-08-27	SN Ia	2
12781	2006er	0.08	5.40656	−1.00997	2006-08-27	SN Ia	1
12782	2006fq	0.07	5.00338	−0.62497	2006-08-27	SN II	1
12819	2006ho	0.11	8.36686	−0.32024	2006-08-29	SN II	1
12820	2006fg	0.04	9.58353	−0.29499	2006-08-29	SN II	4
12841	2006gk	0.29	−38.65275	−1.03367	2006-09-11	SN Ia	1
12842	2006ez	0.09	−36.54476	−1.01596	2006-09-11	SN II	4
12843	2006fa	0.17	−36.12191	−0.98027	2006-09-11	SN Ia	2
12851	2006gm	0.25	−15.21893	−0.62737	2006-09-11	SN Ia	1
12853	2006ey	0.17	−43.23444	+0.72307	2006-09-11	SN Ia	1
12855	2006fk	0.17	−29.74447	+0.71624	2006-09-11	SN Ia	2
12856	2006fl	0.17	−27.13453	+0.75598	2006-09-11	SN Ia	1
12860	2006fc	0.12	−36.30580	+1.17591	2006-09-11	SN Ia	2
12869	2006ge	0.28	−32.60088	+0.00108	2006-09-12	SN Ia	1
12874	2006fb	0.24	−6.03538	−0.17711	2006-09-12	SN Ia	1
12881	2006gu	0.24	10.16235	−0.07357	2006-09-12	SN Ia	1
12883	2006fr	0.31	−47.37411	+0.39867	2006-09-12	SN Ia?	1
12897	2006eb	0.02	18.42139	−0.10158	2006-09-12	SN Ia	1
12898	2006fw	0.08	26.79308	−0.14696	2006-09-12	SN Ia	3
12907	2006fv	0.13	20.40784	+0.41453	2006-09-12	SN Ia?	1
12927	2006fj	0.19	41.78614	+0.77513	2006-09-12	SN Ia	1
12928	2006ew	0.14	−54.99097	−0.97569	2006-09-12	SN Ia	1
12930	2006ex	0.15	−50.31722	−0.47453	2006-09-12	SN Ia	1
12950	2006fy	0.08	−8.33255	−0.84028	2006-09-12	SN Ia	2
12971	2006ff	0.23	6.64850	−0.30207	2006-09-12	SN Ia	1
12972	2006ft	0.26	7.95859	−0.38296	2006-09-12	SN Ia	1
12977	2006gh	0.25	13.69561	−0.25086	2006-09-12	SN Ia	1
12979	2006gf	0.12	11.60148	+0.00348	2006-09-12	SN Ia	1
12983	2006gl	0.27	16.45878	+0.14480	2006-09-12	SN Ia	1
12991	2006gd	0.15	17.60995	−1.06803	2006-09-12	SN II	1
13005	2006fh	0.12	27.39546	−0.64988	2006-09-12	SN Ia	1
13025	2006fx	0.22	−18.43267	+0.41590	2006-09-15	SN Ia	2
13038	2006gn	0.10	−12.17322	+0.50461	2006-09-15	SN Ia	1
13044	2006fm	0.12	−27.45725	+0.50326	2006-09-15	SN Ia	3
13045	2006fn	0.18	−14.97506	+0.53767	2006-09-15	SN Ia	1
13070	2006fu	0.20	−2.21494	−0.74634	2006-09-15	SN Ia	1
13072	2006fi	0.23	−25.04053	+0.02437	2006-09-15	SN Ia	2
13099	2006gb	0.27	−0.18127	−1.25038	2006-09-16	SN Ia	1
13135	2006fz	0.10	4.17229	−0.42454	2006-09-16	SN Ia	9
13136	2006go	0.37	6.14068	−0.27906	2006-09-16	SN Ia	1
13152	2006gg	0.20	7.05211	+0.11801	2006-09-16	SN Ia	1
13174	2006ga	0.24	13.23469	+0.44786	2006-09-16	SN Ia	2
13195	2006fo	0.02	38.16203	+0.61751	2006-09-16	SN Ic	11

Table 6—Continued

Candidate ID[a]	IAU Name	z[b]	RA[c] (degrees in J2000)	Dec	Discovery Date	Type[d]	# of Spectra[e]
13254	2006gx	0.18	42.05867	−0.34703	2006-09-16	SN Ia	1
13305	2006he	0.21	−28.89951	+0.69121	2006-09-17	SN Ia	1
13327	2006jf	0.28	−21.27261	+0.00204	2006-09-17	SN Ia	1
13354	2006hr	0.16	27.56482	−0.88727	2006-09-17	SN Ia	1
13355	2006kh	0.06	27.29935	−0.60526	2006-09-17	SN II	1
13357	2006gw	0.33	29.47294	−0.53415	2006-09-17	SN Ia	1
13370	2006gv	0.20	27.15155	+0.32822	2006-09-18	SN Ia	1
13376	2006gq	0.07	26.30225	+0.35644	2006-09-18	SN II	4
13425	2006gp	0.21	−21.45832	+0.05499	2006-09-18	SN Ia	1
13449	2006ix	0.08	−0.19154	−0.31104	2006-09-18	SN II	1
13467	2006hq	0.07	−5.05354	+0.20523	2006-09-18	SN Ia?	1
13506	2006hg	0.24	25.24334	−0.72785	2006-09-19	SN Ia	1
13511	2006hh	0.24	40.61235	−0.79412	2006-09-19	SN Ia	1
13518	2006mn[g]	···	16.95163	−0.10984	2006-09-19	SN Ia	···
13577	2006kg	0.23	16.07075	+0.76913	2006-09-19	SN II	1
13578	2006hc	0.20	17.39470	+0.70416	2006-09-19	SN Ia	1
13610	2006hd	0.30	−33.98522	+0.72628	2006-09-19	SN Ia	1
13641	2006hf	0.22	−14.78127	−0.98114	2006-09-19	SN Ia	1
13655	2006hs	0.26	39.02022	−0.99418	2006-09-19	SN Ia	1
13727	2006hj	0.23	−42.41192	+0.93262	2006-09-20	SN Ia	2
13736	2006hv	0.15	−23.16671	+1.03097	2006-09-20	SN Ia	2
13757	2006hk	0.28	−9.87691	−1.15785	2006-09-20	SN Ia	1
13796	2006hl	0.15	−9.30843	+0.53288	2006-09-20	SN Ia	3
13830	2006hm	0.33	−8.43828	−0.38228	2006-09-20	SN Ia	1
13835	2006hp	0.25	6.05964	−0.24826	2006-09-20	SN Ia	1
13894	2006jh	0.13	1.69061	−0.03676	2006-09-22	SN Ia	1
13934	2006jg	0.33	−17.88899	−0.43527	2006-09-22	SN Ia	1
13936	2006hz	0.23	3.17083	−0.53548	2006-09-22	SN II	1
13956	2006hi	0.26	20.94181	+0.81673	2006-09-23	SN Ia	1
14019	2006ki	0.22	−43.35758	−0.64795	2006-09-27	SN Ia	1
14024	2006ht	0.20	−41.80144	+0.91635	2006-09-27	SN Ia	1
14108	2006hu	0.14	53.59465	−1.12321	2006-09-28	SN Ia	1
14157	2006kj	0.21	51.13669	+1.02236	2006-09-28	SN Ia?	1
14212	2006iy	0.20	−29.52989	+1.04501	2006-09-29	SN Ia	1
14261	2006jk	0.29	−31.75960	+0.25379	2006-09-29	SN Ia	1
14279	2006hx	0.04	18.48878	+0.37167	2006-09-29	SN Ia	6
14284	2006ib	0.18	49.04929	−0.60094	2006-09-29	SN Ia	1
14298	2006jj	0.27	−45.10495	+1.22326	2006-09-29	SN Ia	1
14318	2006py	0.06	−19.57480	−0.13692	2006-09-30	SN Ia	3
14331	2006kl	0.22	7.88868	−0.13581	2006-09-30	SN Ia	1
14377	2006hw	0.14	48.26431	−0.47163	2006-09-30	SN Ia	1
14397	2006kk	0.39	6.91610	+0.64951	2006-09-30	SN Ia	1
14421	2006ia	0.17	31.82988	+1.25208	2006-09-30	SN Ia	1
14437	2006hy	0.14	−27.91904	−1.19639	2006-10-01	SN Ia	2
14450	2006kn	0.12	−45.47827	+0.90048	2006-10-01	SN II	1

Table 6—Continued

Candidate ID[a]	IAU Name	z[b]	RA[c] (degrees in J2000)	Dec	Discovery Date	Type[d]	# of Spectra[e]
14451	2006ji	0.18	−51.80505	+0.92707	2006-10-01	SN Ia	1
14456	2006jm	0.33	−16.44890	+1.05066	2006-10-01	SN Ia	1
14481	2006lj	0.24	2.68173	+0.20131	2006-10-01	SN Ia	1
14492	2006jo	0.08	20.81130	−0.32964	2006-10-01	SN Ib	2
14599	2006jl	0.05	−51.98055	−0.57454	2006-10-01	SN II	4
14735	2006km	0.30	35.15803	+0.34838	2006-10-02	SN Ia	1
14782	2006jp	0.16	−45.76575	−0.27904	2006-10-02	SN Ia	1
14815	2006iz	0.14	−40.92836	+0.55949	2006-10-03	SN Ia	3
14816	2006ja	0.11	−23.28370	+0.50606	2006-10-03	SN Ia	3
14846	2006jn	0.23	7.66324	+0.14158	2006-10-03	SN Ia	1
14871	2006jq	0.11	54.27710	+0.00936	2006-10-03	SN Ia	3
14979	2006jr	0.18	54.94643	+0.99282	2006-10-03	SN Ia	1
14984	2006js	0.19	−46.16643	−0.09279	2006-10-03	SN Ia	1
15002	2006ko	0.38	22.24981	+0.76995	2006-10-04	SN Ia?	1
15009	2006kp	0.29	32.79856	+0.69583	2006-10-04	SN Ia?	1
15031	2006iw	0.03	−9.66882	+0.25973	2006-10-04	SN II	5
15057	2006md[g]	...	17.88126	0.40949	2006-10-04	SN Ia	...
15129	2006kq	0.20	−41.09761	−0.32143	2006-10-04	SN Ia	1
15132	2006jt	0.14	−30.29977	+0.19769	2006-10-04	SN Ia	2
15136	2006ju	0.15	−8.83745	−0.71836	2006-10-05	SN Ia?	1
15161	2006jw	0.25	35.84291	+0.81900	2006-10-12	SN Ia?	1
15170	2006jx	0.25	58.05858	+0.29207	2006-10-12	SN Ib	1
15171	2006kb	0.12	−55.20746	−1.06449	2006-10-13	SN Ia	2
15201	2006ks	0.21	−22.48059	+0.00364	2006-10-13	SN Ia	1
15203	2006jy	0.20	15.73471	+0.18309	2006-10-13	SN Ia	1
15213	2006lk	0.31	53.01914	−0.10014	2006-10-13	SN Ia	1
15217	2006jv	0.37	22.63421	+0.21980	2006-10-13	SN Ia	1
15219	2006ka	0.25	34.61115	+0.22669	2006-10-13	SN Ia	1
15222	2006jz	0.20	2.85338	+0.70274	2006-10-13	SN Ia	1
15229	2006kr	0.22	4.83198	+1.09072	2006-10-13	SN Ia	1
15234	2006kd	0.13	16.95834	+0.82820	2006-10-13	SN Ia	2
15254	2006oy	0.20	−46.50709	−0.36005	2006-10-14	SN Ia	1
15259	2006kc	0.22	−22.45580	−0.40782	2006-10-14	SN Ia	1
15286	... [g]	0.00	−56.60836	−1.11915	2006-10-15	SN Ia	...
15287	2006kt	0.23	−36.04032	−1.05743	2006-10-15	SN Ia	1
15301	2006lo	0.18	−36.42008	+0.58911	2006-10-15	SN Ia	1
15320	2006kv	0.06	0.77773	+0.91377	2006-10-16	SN II	4
15339	2006ns	0.12	−36.61574	+0.78484	2006-10-17	SN II	4
15340	2006mu	0.14	−23.99717	+0.82135	2006-10-17	SN Ia?	1
15354	2006lp	0.22	6.77368	−0.12598	2006-10-17	SN Ia	2
15356	2006lm	0.28	−24.94668	+0.40995	2006-10-17	SN Ia	1
15365	2006ku	0.19	−5.44334	+1.24909	2006-10-18	SN Ia	1
15369	2006ln	0.24	−11.16705	−0.56261	2006-10-18	SN Ia	2
15383	2006lq	0.32	34.14953	−0.15516	2006-10-18	SN Ia	1
15421	2006kw	0.18	33.74160	+0.60251	2006-10-21	SN Ia	1

Table 6—Continued

Candidate ID[a]	IAU Name	z[b]	RA[c] (degrees in J2000)	Dec	Discovery Date	Type[d]	# of Spectra[e]
15425	2006kx	0.16	55.56108	+0.47829	2006-10-21	SN Ia	1
15433	2006mt	0.22	14.87963	−0.25651	2006-10-21	SN Ia	2
15440	2006lr	0.26	39.72067	+0.09013	2006-10-21	SN Ia	1
15443	2006lb	0.18	49.86744	−0.31803	2006-10-21	SN Ia	1
15453	2006ky	0.18	−40.33170	−1.02429	2006-10-21	SN Ia	1
15456	2006ll	0.38	−28.13274	−0.90341	2006-10-21	SN Ia	1
15459	2006la	0.12	−19.29859	−0.90175	2006-10-21	SN Ia	1
15461	2006kz	0.18	−33.15252	−0.49468	2006-10-21	SN Ia	1
15466	2006mz	0.25	−42.35496	−0.12322	2006-10-21	SN Ia	1
15475	2006lc	0.02	−18.89802	−0.16487	2006-10-21	SN Ic	7
15504	2006oc	0.27	−14.29855	−0.87642	2006-10-22	SN Ia	1
15508	2006ls	0.14	27.16898	−0.57661	2006-10-22	SN Ia	3
15557	2006oz	0.00	−27.77686	+0.89735	2006-10-23	SN Ib	1
15583	2006mv	0.17	37.73108	+0.94630	2006-10-23	SN Ia	1
15584	2006nt	0.28	43.49546	+0.98696	2006-10-23	SN Ia	1
15648	2006ni	0.17	−46.28162	−0.19482	2006-10-23	SN Ia	1
15674	2006nu	0.20	−19.17084	+0.26291	2006-10-23	SN Ia	1
15704	2006nh	0.36	40.21073	+0.65875	2006-10-24	SN Ia	1
15734	2006ng	0.40	5.53028	−0.09564	2006-10-24	SN Ia	1
15749	2006mw	0.12	51.28531	−0.04058	2006-10-24	SN Ia?	1
15756	2006nf	0.39	0.37483	+0.27597	2006-10-24	SN Ia	1
15760	2006mh[g]	···	18.80583	0.39925	2006-10-24	SN Ia	···
15776	2006na	0.32	32.82944	−0.99826	2006-10-24	SN Ia	1
15833	2006mx	0.13	−59.13613	+0.57021	2006-10-26	SN Ia?	1
15868	2006pa	0.25	38.09980	−0.71358	2006-10-28	SN Ia?	3
15872	2006nb	0.21	36.72250	−0.32781	2006-10-28	SN Ia	1
15897	2006pb	0.17	11.68145	−1.03290	2006-10-29	SN Ia	1
15901	2006od	0.17	31.97630	−0.53539	2006-10-29	SN Ia	1
16000	2006nj	0.40	21.11762	+0.07439	2006-10-30	SN Ia	1
16021	2006nc	0.12	13.84373	−0.38881	2006-10-30	SN Ia	2
16032	2006nk	0.20	44.06922	−0.41077	2006-10-30	SN Ia	1
16069	2006nd	0.13	−18.75392	−1.00660	2006-10-31	SN Ia	4
16072	2006nv	0.29	3.12444	−0.97731	2006-10-31	SN Ia	1
16073	2006of	0.16	8.10776	−1.05400	2006-10-31	SN Ia	1
16087	2006pc	0.06	26.04409	−0.15589	2006-11-01	SN II	1
16093	2006oe	0.34	−9.63753	+1.13248	2006-11-01	SN Ia	1
16099	2006nn	0.20	26.42094	−1.05439	2006-11-01	SN Ia	1
16100	2006nl	0.19	30.43629	−1.03241	2006-11-01	SN Ia	1
16106	2006no	0.25	−27.91065	−1.14878	2006-11-01	SN Ia	1
16108	2006og	0.16	−56.98224	+0.57061	2006-11-01	SN Ia	1
16116	2006oh	0.16	−4.69799	−1.10581	2006-11-01	SN Ia	1
16165	2006nw	0.16	30.73314	−0.53387	2006-11-02	SN Ia	1
16179	2006nx	0.14	53.37764	−0.67729	2006-11-03	SN Ic	6
16185	2006ok	0.10	16.86807	−0.26937	2006-11-09	SN Ia	1
16192	2006ny	0.08	9.82211	+0.08393	2006-11-09	SN II	2

Table 6—Continued

Candidate ID[a]	IAU Name	z[b]	RA[c] (degrees in J2000)	Dec	Discovery Date	Type[d]	# of Spectra[e]
16206	2006pe	0.16	5.78819	−0.05363	2006-11-09	SN Ia	1
16211	2006nm	0.31	−11.83591	+0.26693	2006-11-09	SN Ia	1
16213	2006oi	0.20	8.97105	+0.25840	2006-11-09	SN Ia	1
16215	2006ne	0.05	18.40767	+0.42388	2006-11-09	SN Ia	8
16232	2006oj	0.34	17.20541	−0.98955	2006-11-10	SN Ia	1
16259	2006ol	0.12	−7.97003	+0.85635	2006-11-10	SN Ia	1
16276	2006om	0.16	20.57866	+1.01062	2006-11-10	SN Ia	1
16280	2006nz	0.04	14.12170	−1.22673	2006-11-11	SN Ia	4
16281	2006pd	0.19	−7.05785	−0.66805	2006-11-11	SN Ia	1
16287	2006np	0.11	46.66451	+0.06403	2006-11-11	SN Ia	6
16314	2006oa	0.06	−39.07107	−0.84347	2006-11-12	SN Ia	3
16333	2006on	0.07	−31.00630	−1.07020	2006-11-12	SN Ia	3
16350	2006ph	0.24	−36.36051	−0.88583	2006-11-14	SN Ia	1
16352	2006pk	0.25	−13.75064	−0.87336	2006-11-14	SN Ia	2
16357	2006pi	0.37	−29.18082	−0.60684	2006-11-14	SN Ia	1
16392	2006ob	0.06	27.95060	+0.26331	2006-11-14	SN Ia	6
16402	2006sv	0.30	−23.63228	+0.26527	2006-11-14	SN Ia	2
16414	2006pj	0.31	−20.67354	+0.73814	2006-11-14	SN Ia	1
16421	2006pg	0.32	51.83630	+1.08966	2006-11-14	SN Ia	1
16442	2006oo	0.28	−30.05319	−0.73322	2006-11-15	SN Ia	1
16473	2006pl	0.22	−31.38785	+0.58852	2006-11-15	SN Ia	2
16482	2006pm	0.20	−31.29049	+0.93367	2006-11-15	SN Ia	1
16541	2006pn	0.13	57.26188	−0.53277	2006-11-16	SN Ia	1
16567	2006pf	0.40	25.43805	−0.18915	2006-11-17	SN Ia	1
16578	2006po	0.18	−54.18680	−0.84849	2006-11-17	SN Ia	1
16618	2006pq	0.20	21.27937	−1.21894	2006-11-18	SN Ia	1
16619	2006ps	0.10	25.93874	−1.11192	2006-11-18	SN Ia	2
16631	2006pv	0.21	54.62279	−0.67557	2006-11-18	SN Ia	1
16641	2006pr	0.11	23.56123	−0.40363	2006-11-18	SN Ia	3
16644	2006pt	0.30	36.81737	−0.39348	2006-11-18	SN Ia	1
16668	2006pu	0.15	40.72425	+0.89287	2006-11-18	SN II	1
16692	2006op	0.03	−39.61722	+0.99331	2006-11-18	SN Ia?	2
16737	2006qc	0.20	−47.16732	−0.95232	2006-11-20	SN Ia	1
16748	2006sx	0.23	7.95132	−0.51394	2006-11-20	SN Ia	2
16758	2006pw	0.33	−18.38765	+1.15081	2006-11-20	SN Ia	1
16774	2006sy	0.21	35.27168	+0.82840	2006-11-20	SN Ia	2
16776	2006qd	0.27	−12.97859	−0.17608	2006-11-20	SN Ia	1
16779	2006qa	0.40	45.29054	−0.02624	2006-11-20	SN Ia	1
16781	2006qb	0.33	52.06103	−0.20096	2006-11-20	SN Ia	1
16789	2006pz	0.33	43.78434	+0.23477	2006-11-20	SN Ia	1
16793	2006qg	0.23	−31.42464	+0.44701	2006-11-20	SN Ia	1
16836	2006sw	0.33	16.25085	−0.37464	2006-11-21	SN Ia	1
16840	2006qf	0.17	57.98849	−0.39658	2006-11-21	SN II	1
16847	2006px	0.28	−6.67875	+0.96110	2006-11-21	SN Ia	1
16872	2006qh	0.12	−33.02908	+0.70684	2006-11-21	SN Ia	1

Table 6—Continued

Candidate ID[a]	IAU Name	z[b]	RA[c] (degrees in J2000)	Dec	Discovery Date	Type[d]	# of Spectra[e]
16894	2006tb	0.30	56.31453	−0.12854	2006-11-22	SN Ia	1
16899	2006ta	0.29	52.46008	+0.29509	2006-11-22	SN Ia	1
16938	2006qe	0.39	−11.91674	−0.53442	2006-11-22	SN Ia	1
16941	2006sz	0.19	−4.28142	−0.55636	2006-11-22	SN Ia?	1
16953	2006pp	0.34	12.24364	+0.47695	2006-11-23	SN Ia	1
16956	2006qj	0.11	−57.22662	−0.31996	2006-11-23	SN Ia	1
16988	2006qk	0.06	−23.61507	+0.15419	2006-11-24	SN Ic	4
17048	2006qi	0.19	27.58151	+0.88490	2006-11-24	SN Ia	1
17081	2006ql	0.27	27.53797	+0.42048	2006-11-25	SN Ia	1
17106	2006tc	0.21	47.00818	+0.94343	2006-11-25	SN Ia	1
17117	2006qm	0.14	40.60031	−0.79652	2006-11-25	SN Ia	2
17135	2006rz	0.03	56.52825	+0.38975	2006-11-26	SN Ia	4

[a]Internal SN candidate designation.

[b]Preliminary spectroscopic redshifts. The typical uncertainties are ~ 0.01.

[c]Right Ascension is provided in decimal degrees defined in the range [-180°,+180°].

[d]The preliminary spectroscopic type of the SN candidate. Spectroscopically probable SNe Ia are designated "SN Ia?" (see Zheng et al. 2007).

[e]This includes all spectral observations performed including those of the SN candidate and possibly its host galaxy.

[f]Spectroscopically confirmed by the CfA SN Group.

[g]Spectroscopically confirmed by the ESSENCE Group.

Table 7. Summary of the 2005 and 2006 search seasons

Number of	2005	2006
Nights on SDSS 2.5m	59	60
Runs	73	90
Total number of objects	375,187	391,435
Number of objects scanned	155,616	14,430
Number of objects tagged as SN	24,402	4,189
SN candidates discovered[a]	11,385	3,694
Single-epoch candidates[b]	6,618	599

[a]The number of unique SN candidates tagged by a scanner. This number differs from the number of objects tagged as a SN because it includes multiple objects from the same candidate.

[b]Candidates that were detected in only a single run. Most of these sources are likely to be solar system objects.

Table 8. Spectroscopic Observations of 2005 and 2006 Candidates

Number of Spectroscopic Observations	2005	2006
SN Ia candidates[a]	173	241
Identified as SN Ia	130[b]	197[c]
Identified as probable SN Ia	16	14
Resulting in host galaxy spectra of photometric SN Ia	7	7
Resulting in other host galaxy spectra	3	6
Identified as SN Ib/c	1	0
Identified as SN II	5[d]	6
Identified as AGN	2	0
Identified as flaring M-dwarf	1	1
Unidentified	8	10
Non-SN Ia candidates[e]	24	42
Identified as SN Ib/c	7	6
Identified as SN II	7	14
Photometric SN Ia candidates with host galaxy spectroscopy[f]	81	6
Other SN candidates with host galaxy spectroscopy[g]	26	0
Duplicate and multi-epoch spectra[h]	86	148
Total	390	437

[a]Number of candidates targeted for spectroscopy that had been photometrically identified as a possible SN Ia.

[b]This includes one SN Ia that was spectroscopically confirmed by the Texas Supernova Search (Quimby et al. 2007).

[c]This includes five SNe Ia that were spectroscopically confirmed by the CfA SN Group and the ESSENCE Group.

[d]This includes one SN II that was spectroscopically confirmed by the ESSENCE Group.

[e]This includes observations of core-collapse SNe, novae, and other interesting transients.

[f]Of the 113 host galaxy spectra obtained, the measured redshifts of a sample of 81 sources were consistent with the photometric redshift estimated from the SN Ia model light curve fits, and were thus identified as photometric SN Ia.

[g]These were targeted as host galaxies of photometric SN Ia candidates. The observations, however, resulted in either noisy, unclassifiable spectra or measured spectroscopic redshifts that are inconsistent with the SN Ia light curve redshifts implying that the candidates are not SNe Ia.

[h]The total number of duplicate and multi-epoch spectra; not the number of candidates targeted for multi-epoch spectroscopy.